

New Theobromine Apoptotic Analogue with Anticancer Potential Targeting the EGFR Protein: Computational and *In Vitro* Studies

Ibrahim H. Eissa, Reda G. Yousef, Eslam B. Elkaeed, Aisha A. Alsouk, Dalal Z. Husein, Ibrahim M. Ibrahim, Ahmed Ismail, Hazem Elkady,* and Ahmed M. Metwaly*



Cite This: *ACS Omega* 2024, 9, 15861–15881



Read Online

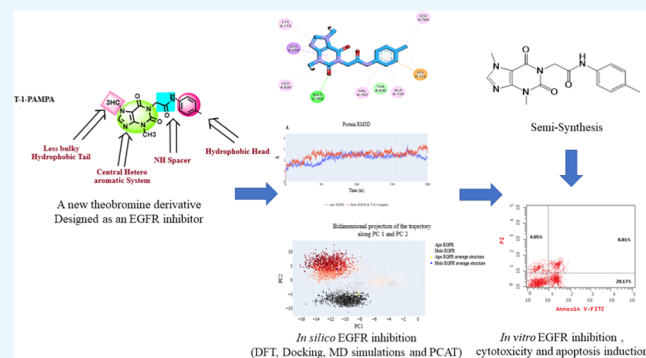
ACCESS |

Metrics & More

Article Recommendations

Supporting Information

ABSTRACT: Aim: The aim of this study was to design and examine a novel epidermal growth factor receptor (EGFR) inhibitor with apoptotic properties by utilizing the essential structural characteristics of existing EGFR inhibitors as a foundation. Method: The study began with the natural alkaloid theobromine and developed a new semisynthetic derivative (**T-1-PMPA**). Computational ADMET assessments were conducted first to evaluate its anticipated safety and general drug-likeness. Deep density functional theory (DFT) computations were initially performed to validate the three-dimensional (3D) structure and reactivity of **T-1-PMPA**. Molecular docking against the EGFR proteins was conducted to investigate **T-1-PMPA**'s binding affinity and inhibitory potential. Additional molecular dynamics (MD) simulations over 200 ns along with MM-GPSA, PLIP, and principal component analysis of trajectories (PCAT) experiments were employed to verify the binding and inhibitory properties of **T-1-PMPA**. Afterward, **T-1-PMPA** was semisynthesized to validate the proposed design and *in silico* findings through several *in vitro* examinations. Results: DFT studies indicated **T-1-PMPA**'s reactivity using electrostatic potential, global reactive indices, and total density of states. Molecular docking, MD simulations, MM-GPSA, PLIP, and ED suggested the binding and inhibitory properties of **T-1-PMPA** against the EGFR protein. The *in silico* ADMET predicted **T-1-PMPA**'s safety and general drug-likeness. *In vitro* experiments demonstrated that **T-1-PMPA** effectively inhibited EGFR^{WT} and EGFR^{T90M}, with IC₅₀ values of 86 and 561 nM, respectively, compared to Erlotinib (31 and 456 nM). **T-1-PMPA** also showed significant suppression of the proliferation of HepG2 and MCF7 malignant cell lines, with IC₅₀ values of 3.51 and 4.13 μM, respectively. The selectivity indices against the two cancer cell lines indicated the overall safety of **T-1-PMPA**. Flow cytometry confirmed the apoptotic effects of **T-1-PMPA** by increasing the total percentage of apoptosis to 42% compared to 31, and 3% in Erlotinib-treated and control cells, respectively. The qRT-PCR analysis further supported the apoptotic effects by revealing significant increases in the levels of Casp3 and Casp9. Additionally, **T-1-PMPA** controlled the levels of TNFα and IL2 by 74 and 50%, comparing Erlotinib's values (84 and 74%), respectively. Conclusion: In conclusion, our study's findings suggest the potential of **T-1-PMPA** as a promising apoptotic anticancer lead compound targeting the EGFR.



1. INTRODUCTION

Cancer remains a significant global cause of death, despite extensive scientific research and clinical trials of promising new medicines.¹ The development of an efficient tailored chemotherapeutic drug poses a significant challenge for medicinal chemists.² Within our cells, apoptosis, a critical cellular process, acts as a safeguard against cancer development by eliminating damaged or malignant cells in response to various oncogenic stresses, such as uncontrolled cell growth or DNA damage.³ Apoptosis also plays a role in suppressing tumorigenesis through multiple mechanisms, including the removal of oncogenic proteins and the modulation of cellular signaling pathways.⁴ Notably, the epidermal growth factor receptor (EGFR) has been closely linked to apoptosis in cancer cells.^{5,6} Furthermore, EGFR contributes significantly to the develop-

ment and progression of various types of carcinomas.^{7–9} Increased expression of EGFR promotes cell proliferation, differentiation, and survival.¹⁰ Remarkably, elevated levels of EGFR expression have been associated with lower survival rates across different cancer types, underscoring its value as a potent prognostic indicator.¹¹

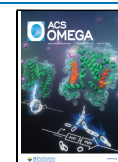
In addition to the discovery and repurposing of potent drugs, studying the structure–activity relationships can

Received: October 17, 2023

Revised: March 6, 2024

Accepted: March 12, 2024

Published: March 27, 2024



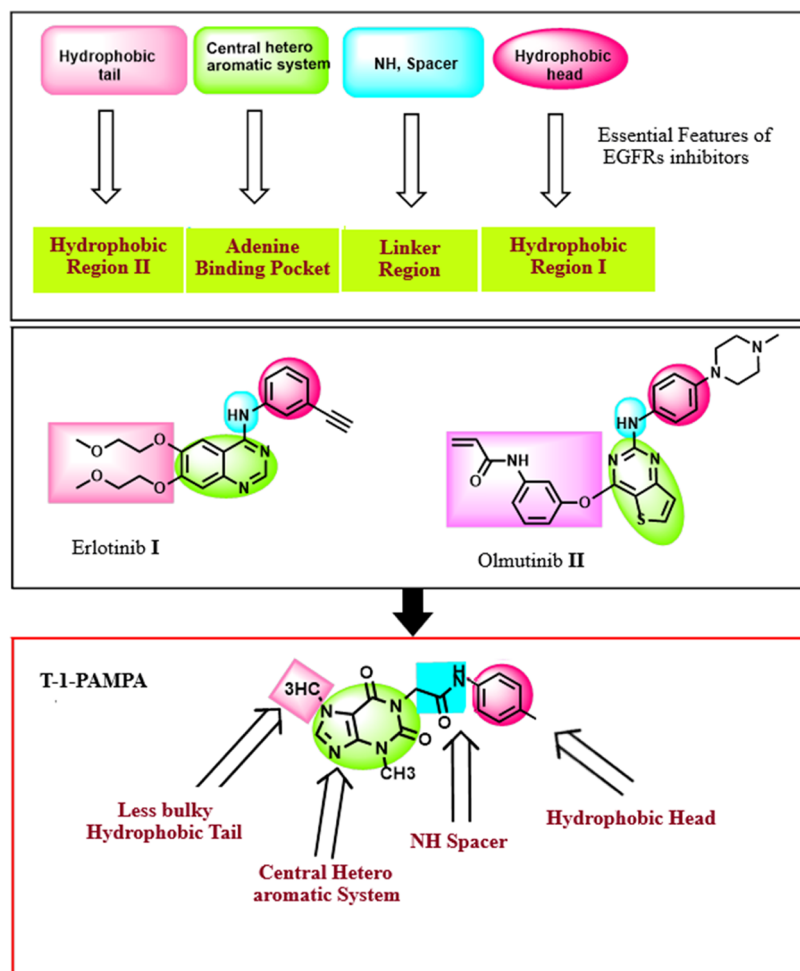


Figure 1. T-1-PMPA's design rationale.

enhance the drug-likeness, pharmacokinetics, and pharmacodynamics of novel therapeutic agents.¹² Computational chemistry employing a variety of techniques and software enables the investigation of interactions between potential drugs and biomolecules. This field has found wide-ranging applications in the pharmaceutical industry.^{13–15} Over the years, numerous computational chemistry applications have been developed, including molecular and drug design,^{16,17} docking simulations,¹⁸ ligand-based approaches such as ADMET,¹⁹ density functional theory (DFT),²⁰ structure similarity,²¹ and pharmacophore assessment.²²

Our team's ongoing quest is to discover compounds that have the potential to combat cancer by targeting the EGFR protein.^{23–29}

Erlotinib I³⁰ and olmutinib II³¹ are representative examples of EGFR inhibitors that have demonstrated enhanced efficacy against wild-type EGFR^{WT} and mutant EGFR^{T790M}, respectively.

EGFR inhibitors were reported to possess four pharmacophoric features essential for good fitting against the active site of EGFR.³² The features include a heteroaromatic system, an NH spacer, a terminal hydrophobic head, and a hydrophobic tail to engage and bind with the adenine binding pocket, the linker region, and the hydrophobic regions I and II, respectively.^{33–35} Figure 1 illustrates these features, showing avitinib I and olmutinib II as examples of the reported EGFR inhibitors they have. Also, Figure 1 explains that T-1-PMPA

comprises the acquired features as follows: the xanthine moiety represents a flat heteroaromatic system that is essential to engage the adenine binding pocket. Fortunately, the xanthine moiety is familiar to the human physiological system being a natural moiety. Additionally, the acetamide moiety served as an NH spacer (linker). Moreover, 4-methyl phenyl was utilized as a hydrophobic lead to engage the hydrophobic region I. The 4-methyl moiety may increase the hydrophobicity of the designed compound and the possibility of being engaged in hydrophobic interactions. Finally, the methyl group at the 7-position of the xanthine moiety represents a less bulky hydrophobic tail to engage the hydrophobic region II in the active EGFR's pocket. Our research strategy places a strong emphasis on conducting detailed computational studies before synthesis, aligning with our commitment to environmental sustainability, occupational health and safety, efficient resource utilization, and time management. This approach ensures that only the most promising candidates, identified through rigorous computational screening, undergo the synthesis process, contributing to more responsible and impactful research. In this research, we present the newly semi-synthesized and lead compound (T-1-PMPA). The compound exhibits encouraging *in silico* and *in vitro* anticancer properties, indicating its promise as a potential therapeutic agent.

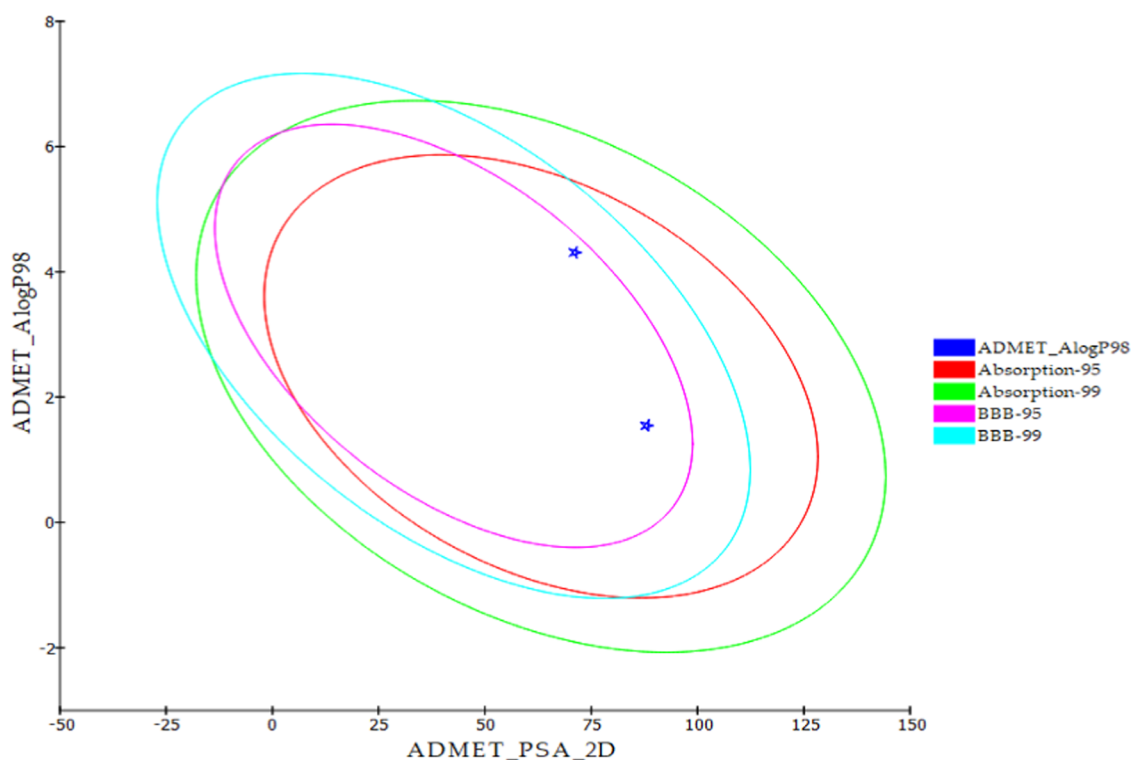


Figure 2. Computational prediction of ADMET parameters for T-1-PMPA and Erlotinib.

Table 1. ADMET Parameters for T-1-PMPA and Erlotinib

| comp | BBB level | solubility | absorption | hepatotoxicity | CYP2D6 | PBP (%) |
|-----------|-----------|------------|------------|----------------|---------------|--------------|
| T-1-PMPA | low | good | good | not toxic | no inhibition | less than 90 |
| Erlotinib | high | low | good | toxic | no inhibition | more than 90 |

2. RESULTS AND DISCUSSION

2.1. Computational Studies. **2.1.1. ADMET Profiling Study.** ADMET prediction, encompassing absorption, distribution, metabolism, excretion, and toxicity, plays a pivotal role in drug discovery. Its importance can be traced back to the introduction of Lipinski's Rule of Five by Dr. Christopher Lipinski. This rule, formulated by Dr. Lipinski, has served as a guiding principle for researchers in identifying compounds with improved drug-like characteristics.³⁶ However, as drug discovery has advanced, the scope of ADMET prediction has also expanded. Presently, it includes a diverse array of techniques and tools such as the development of high-throughput assays, the application of machine learning algorithms, data mining methods, advanced data visualization, and sophisticated structure-based modeling approaches.³⁷

The importance of predictive ADMET cannot be emphasized enough, especially during the early stages of drug development. It acts as a crucial checkpoint, assisting in making informed decisions regarding the advancement of compounds through the drug development pipeline. By evaluating various aspects of a compound, such as its absorption potential into the body, distribution to the targeted tissues, stability during metabolic processes, elimination, and likelihood of causing toxicity, ADMET prediction offers valuable insights into a compound's suitability as a potential drug candidate. As a result, it not only saves resources and valuable time but also mitigates the risk of costly setbacks in

the later stages of development and the need for market withdrawals.³⁸

This study was initiated with ADMET profiling to assess the suitability of T-1-PMPA for drug development. This assessment plays a critical role in deciding whether T-1-PMPA should be explored further and incorporated into our ongoing research plans. Accordingly, we employed Discovery studio to computationally predict the ADMET properties of T-1-PMPA, utilizing Erlotinib as a reference molecule. The comparative analysis of ADMET results between T-1-PMPA and Erlotinib (Figure 2) indicated a favorable degree of drug-likeness. T-1-PMPA was projected to have minimal ability to penetrate the blood–brain barrier (BBB), along with nonhepatotoxic and noninhibitory characteristics toward cytochrome P-450, CYP2D6. Moreover, T-1-PMPA displayed a good aqueous solubility and moderate levels of intestinal absorption, as depicted in Table 1.

2.1.2. In Silico Toxicity Studies. The application of *in silico* methods has emerged as a critical component in the field of drug development due to their ability to reduce the reliance on *in vitro* and *in vivo* experiments, thereby minimizing associated time delays.³⁹ Within the realm of *in silico* toxicity prediction, different kinds of software are employed to compare the fundamental chemical structural characteristics of the molecules under investigation with those of numerous molecules previously classified as safe or toxic. This approach utilizes the structure–activity relationship (SAR)-predictive toxicity method.⁴⁰

Table 2. *In Silico* Toxicity Studies of T-1-PMPA and Erlotinib

| comp. | FDA-C-MF | TD ₅₀ -M ^a | A-M | TD ₅₀ -R ^b | R-O-LD ₅₀ ^b | R-C-LOAEL ^b | DI | OI |
|-----------|---------------|----------------------------------|------------|----------------------------------|-----------------------------------|------------------------|----|------|
| T-1-PMPA | noncarcinogen | 57.0705 | nonmutagen | 0.02795 | 3.06204 | 0.0214464 | no | mild |
| Erlotinib | | 39.7706 | | 0.08279 | 0.662169 | 0.0359487 | | |

^aUnit: mg/kg/day. ^bUnit: g/kg.

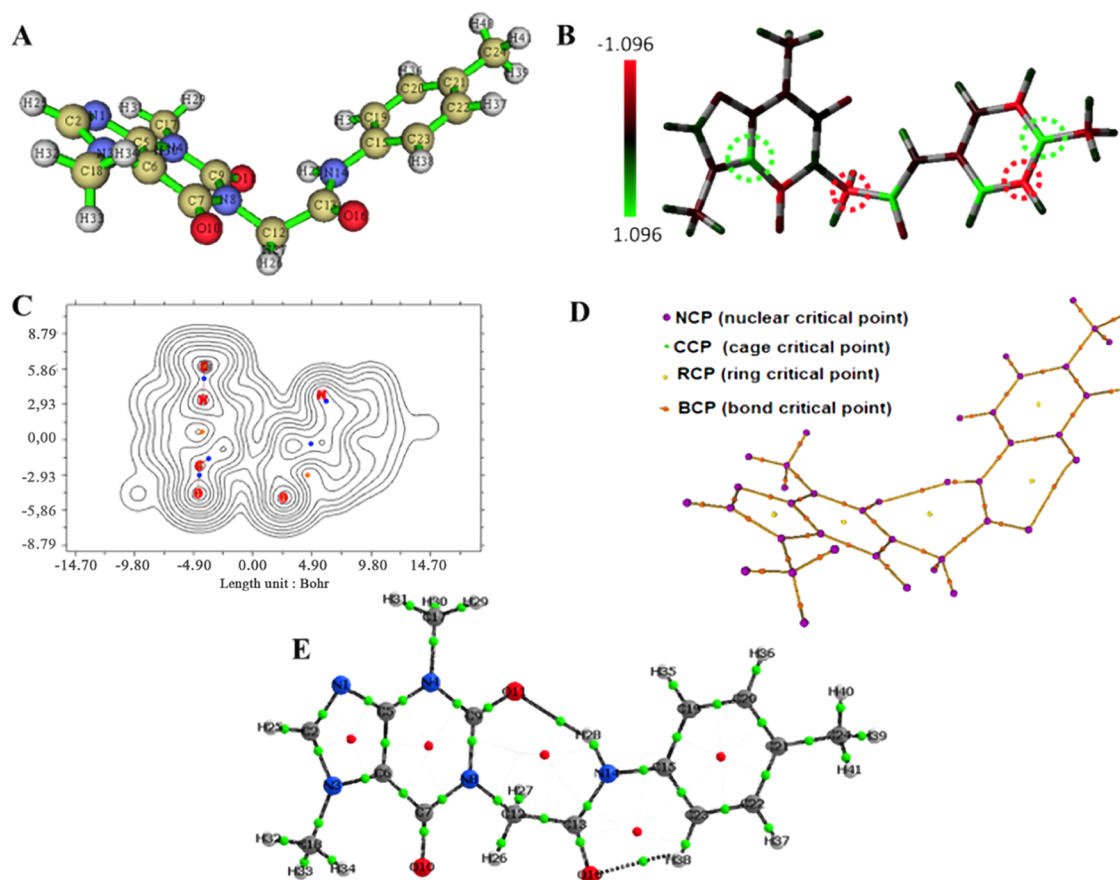


Figure 3. (A) T-1-PMPA's optimized geometry, (B) T-1-PMPA's mulliken atomic charge distribution, (C) T-1-PMPA's QTAIM maps (contour lines), (D) T-1-PMPA's QTAIM maps (1ry intrabonding routes), and (E) T-1-PMPA's QTAIM maps showing bonding critical points (BCPs).

Using Discovery Studio software, we have applied eight toxicity models to assess T-1-PMPA's safety profile. Every model is tailored to address specific facets of toxicity, providing insights into potential risks linked to the compound in different contexts. The utilized models were as follows: FDA Rodent Carcinogenicity in Rat-Female (FDA-C-MF) to evaluate the carcinogenic potential in female rats, aligning with FDA regulatory standards, which aids in determining whether T-1-PMPA may pose long-term cancer risks;⁴¹ Ames Mutagenicity (A-M) to assess c T-1-PMPA's mutagenic potential, particularly its effects on genetic material, which employs the Ames test to evaluate genetic alterations induced by T-1-PMPA;⁴² Mouse Carcinogenicity Median Toxic Dose (TD₅₀-M) to explore T-1-PMPA's potential to induce carcinogenicity in mice;⁴³ Rat Maximum Tolerable Dose (TD₅₀-R) to establish safe dosage levels in preclinical studies, offering information on the upper limits of tolerance;⁴⁴ Rat Oral LD₅₀ (R-O-LD₅₀) to determine the lethal dose at which 50% of tested rats succumb to T-1-PMPA's toxicity when administered orally, essential for assessing acute toxicity;⁴⁵ Rat Chronic LOAEL (R-C-LOAEL) to identify the Lowest Observed Adverse Effect Level, a key parameter in assessing T-1-PMPA's chronic toxicity;⁴⁶ and

Dermal Irritability (DI) and Ocular Irritability (OI) used to understand T-1-PMPA's effects when it contacts the skin or eyes.

By utilizing this extensive range of toxicity models, we acquire a comprehensive perspective on the safety profile of T-1-PMPA. This includes considerations of its potential for carcinogenicity, mutagenicity, lethal dosage thresholds, chronic toxicity, and irritation risks. These insights play a crucial role in making informed decisions about the appropriateness of T-1-PMPA for the advancement of subsequent stages of research. Table 2 shows that T-1-PMPA demonstrated general, highly safe levels in all models. In detail, T-1-PMPA's results were similar to those of Erlotinib in four models and safer results in two models. Only at the TD₅₀-R and R-C-LOAEL models, the safety results of T-1-PMPA were slightly lower than those of Erlotinib. However, the anticipated values are very safe.

2.1.3. DFT. DFT was employed to determine T-1-PMPA's reactivity concerning the target EGFR protein as well as to comprehend its electronic and structural characteristics. Figure 3 displays the optimized structure that was carried out at level DFT/B3LYP/6-311++G (d, p) of theory. According to Table 1, the neutral structure of T-1-PMPA is a singlet made up of

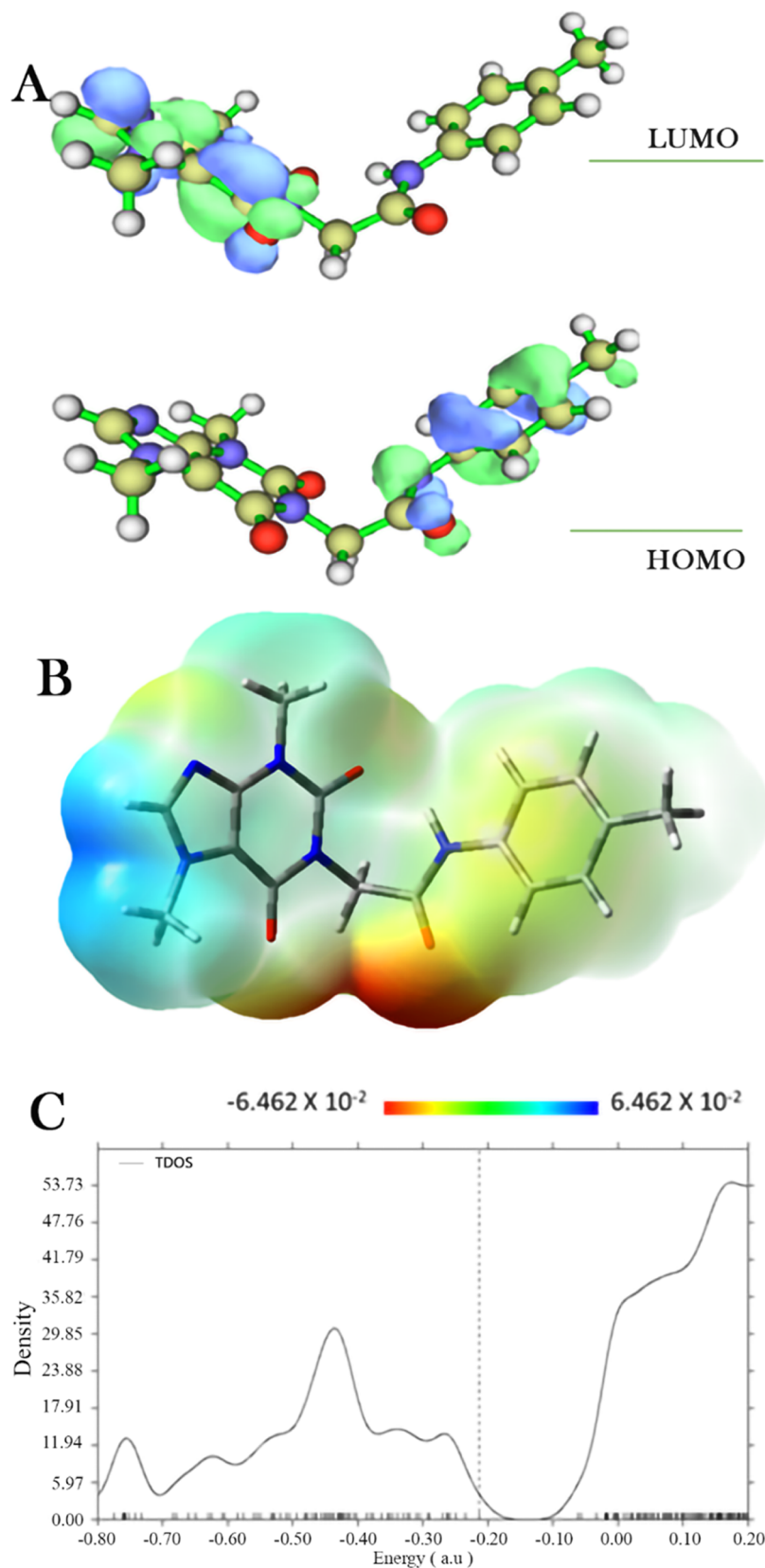


Figure 4. (A) T-1-PMPA's FMO analysis, (B) T-1-PMPA's ESP analysis, and (C), T-1-PMPA's TDOS analysis.

41 atoms, with total ground energy (TE) and dipole moment (Dm) measurements of -30470 eV and 5.94 D, respectively. The high Dm value that was observed may be highly correlated to the inhibitory activity and quantity of hydrogen bonding

donors. Because T-1-PMPA is extremely polar and has a wide separation of charges, it is predicted that it would participate in dipole–dipole interactions, π – π stacking, and hydrogen bonding.

Table 3. DFT Calculated Global Reactivity Parameters for T-1-PMPA

| IP | EA | μ (eV) | χ (eV) | η (eV) | σ (eV) | ω (eV) | Dm (Debye) | TE (eV) | ΔN_{\max} | ΔE (eV) |
|-------|-------|------------|-------------|-------------|---------------|---------------|------------|----------|-------------------|-----------------|
| 5.907 | 1.561 | -3.734 | 3.734 | 2.173 | 0.460 | 15.145 | 5.942 | -30470.0 | 1.719 | -15.145 |

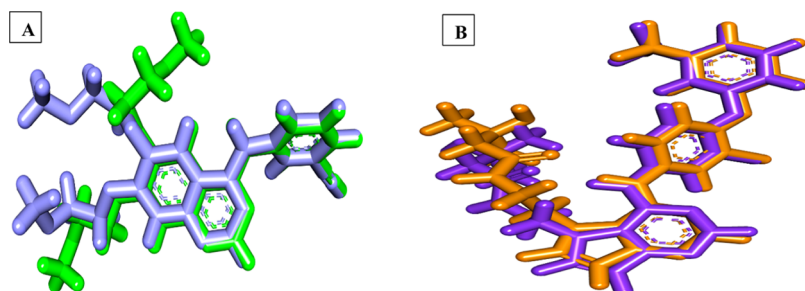


Figure 5. (A) Validation of wild EGFR using Erlotinib as a cocrystallized ligand and (B) validation of mutant EGFR using TAK-285 as a cocrystallized ligand.

Table 4. ΔG and Binding Pattern of Erlotinib and T-1-PMPA against the Wild EGFR (EGFR^{WT})

| Compound | Erlotinib | T-1-PMPA |
|---------------------------------|---------------------------|---|
| 2D Str. in the active pocket | | |
| ΔG | -20.11 kcal/mol | -21.18 kcal/mol |
| No. of H.B/Amino acids involved | 1/Met769 | 1/Met769 |
| No. of H.I/Amino acids involved | 5/ Leu820, Ala719, Val702 | 9/ Cys773, Leu694, Leu820, Leu764, Lys721, Leu820, Ala719, Val702 |
| No. of E.B/Amino acids involved | 1/ Lys721 | 1/ Lys721 |

T-1-PMPA displays a significant charge separation, which is further supported by the Mulliken charge analysis in Figure 3B. All hydrogen atoms have positive charges according to the Mulliken color scale for the 41 component atoms of T-1-PMPA. Due to the strong electronegativity of oxygen atoms, the most positive hydrogens are located adjacent to them. Additionally, in contrast to the other negatively charged carbon atoms, the carbon atoms close to the oxygen atoms have positive charges. Among the most positive carbon atoms are C21 and C6, whereas C12 and C22 are the most negative.

In order to determine atoms in molecules based on electron density, the optimized geometry is examined using the Multiwfn and AIMAll programs. In terms of bonding critical points (BCP) and bonding routes, the quantum theory of atoms in molecules (QTAIM) approach has been used. The

color-filled map with contour lines is in Figure 3C and the primary intrabonding routes are shown in Figure 3D and revealed that T-1-PMPA is bent. Figures 3E, S7 and Table S6 compute and present the QTAIM parameters and detailed critical points. The electron density (ρ) > 0.1 au and the Laplacian ($\nabla^2\rho$) > 0 of the QTAIM parameters suggest intraclosed-shell bonding or noncovalent interactions. The estimated energy density $H(r)$ > 0 and electrostatic bonding are dominant.

Frontiers molecular orbital analysis, specifically the highest occupied molecular orbital (HOMO) and lowest unoccupied molecular orbital (LUMO) energies, was also used to analyze the charge transfer inside T-1-PMPA. Figure 4A shows the distribution of HOMO and LUMO densities, and 4.34 eV was discovered to be the energy between HOMO and LUMO. The

Table 5. ΔG and Binding Pattern of TAK-285 and T-1-PMPA against the Mutant EGFR (EGFR^{T790M})

| Name | TAK-285 | T-1-PMPA |
|----------------------------------|--|---------------------------------------|
| 2D Str. in the active pocket | | |
| ΔG | -18.15 kcal/mol | -17.55 kcal/mol |
| No. of H.Bs/Amino acids involved | 3/ Lys745, Met793, and Ser720 | 2/Met793, Thr854 |
| No. of H.Is/Amino acids involved | 12/ Leu844, Ala743, Leu788, Val726, Ile759, Met790, and Lys745 | 10/ Leu844, Ala743, Leu71, and Met793 |
| No. of E.Bs/Amino acids involved | 2/Met790 and Glu762 | Lys745 |

stable molecule is often distinguished by a high energy gap, E_{gap} , which makes it harder and less reactive. Reactive species are those having a small E_{gap} , which shows that they are less stable and more biologically active. The results demonstrate that T-1-PMPA is a potentially active inhibitor.⁴⁷ The calculated values of the frequently used quantum parameters softness, hardness, electronegativity, and electrophilicity (Table 3) demonstrate that T-1-PMPA is a biologically active member.

For predicting relative chemically active sites for interhydrogen bonding, nucleophilic, and electrophilic attacks, the electrostatic potential (ESP) is helpful. The optimized structure is used to generate the ESP plot for T-1-PMPA, which is shown in Figure 4B. The 3D figure displays blue areas over hydrogen atoms to signify positive electrostatic potential and red color regions over oxygen atoms to indicate negative electrostatic potential. The electrostatic potential in the green zones over the π -system is neutral and forms hydrophobic interactions. Protons are attracted to negative potential zones by electrophilic reactivity, whereas they are repelled by positive potential zones by nucleophilic reactivity.⁴⁸

The largest electron density is located over the orbitals over LUMO, as shown in Figure 4C, according to the prediction of the total density of states (TDOS).

2.1.4. Molecular Docking Studies. **2.1.4.1. Molecular Docking Validation.** The binding mode between T-1-PMPA, wild, and mutant types of EGFR was inspected through a molecular docking study utilizing the MOE2019 protocol. The docking feasibility was corroborated through redocking the native ligands Erlotinib and TAK-285 with the corresponding enzymes (EGFR^{WT}; PDB: 4HJO and EGFR^{T790M}; PDB: 3W2O). The cocrystal conformations reproduced RMSD of 1.44 and 1.14 Å after the redocking, as presented in Figure 5.

2.1.4.2. Molecular Docking against EGFR^{WT}. Matching with reported findings, Erlotinib, a native inhibitor of EGFR^{WT} displayed one key hydrogen bond (H.B.) with Met769 in the adenine pocket. In the hydrophobic pocket, two hydrophobic interactions (H.I) were generated with Ala719 and Val702 in addition to one pi-cation bond with Lys721. T-1-PMPA adopted a compact conformation to fix into the EGFR^{WT} active site (Table 2). It resided in the adenine pocket, where one essential H.B was generated between the 2-oxo group of the purine moiety and Met769 (bond length 2.10 Å). The presence of the *p*-tolyl moiety gave T-1-PMPA the ability to incorporate effectively in the hydrophobic region via numerous interactions. In depth, the *p*-tolyl group generated four pi-pi interactions with Leu764, Lys721, Ala719, and Val702. Also, in the same pocket, one electrostatic bond (E.B.) with Lys721 was observed (Table 4).

2.1.4.3. Molecular Docking against EGFR^{T790M}. TAK-285, a native inhibitor for EGFR^{T790M}, presented a key hydrogen bond with Met793 (2.30 Å) in the adenine pocket through N-1 of the pyrimidine moiety. In the hydrophobic region, 3-(trifluoromethyl)phenoxy and *N*-ethyl-3-hydroxy-3-methylbutanamide moieties were stabilized through hydrophobic bonds with Lys745, Ile759, Met790, Val726, and Leu844 (Table 5).

T-1-PMPA was appended onto the catalytic site of EGFR^{T790M}. The purine moiety achieved two hydrogen bonds with Met793 and Thr854 in addition to eight hydrophobic interactions with Leu844, Ala743, Leu71, and Met793 in the adenine pocket. On the other side, the methyl group of the *p*-tolyl moiety formed two pi-pi bonds with Leu788 and Ile759. Furthermore, the phenyl group had one electrostatic interaction with Lys721 (Table 5).

2.1.5. Molecular Dynamics (MD) Simulations. Molecular dynamics (MD) simulations are advanced computational techniques employed to systematically investigate the dynamic

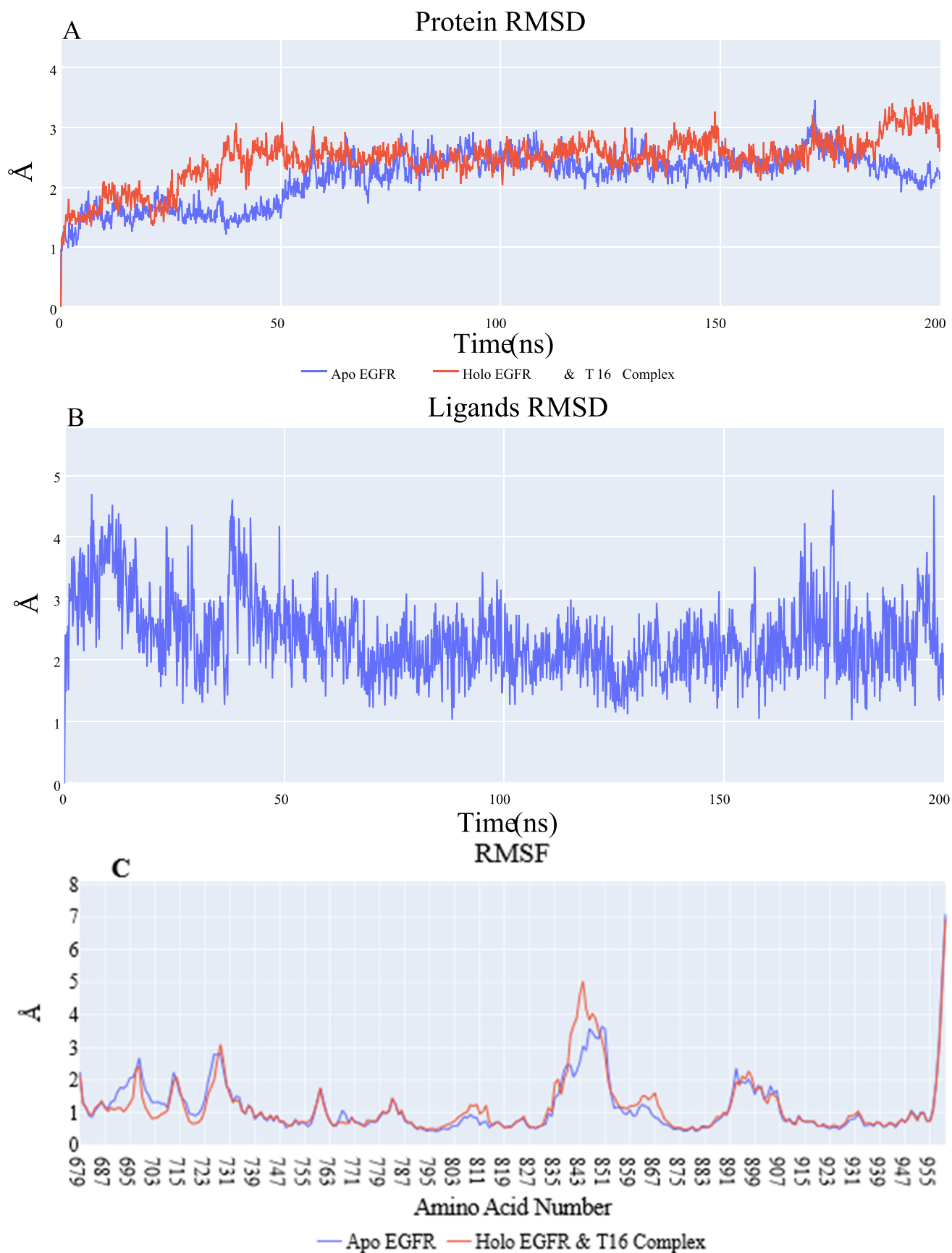


Figure 6. EGFR-T-1-PMPA complex dynamics: (A) EGFR's RMSD, (B) T-1-PMPA's RMSD graph, and (C) EGFR's RMSF graph.

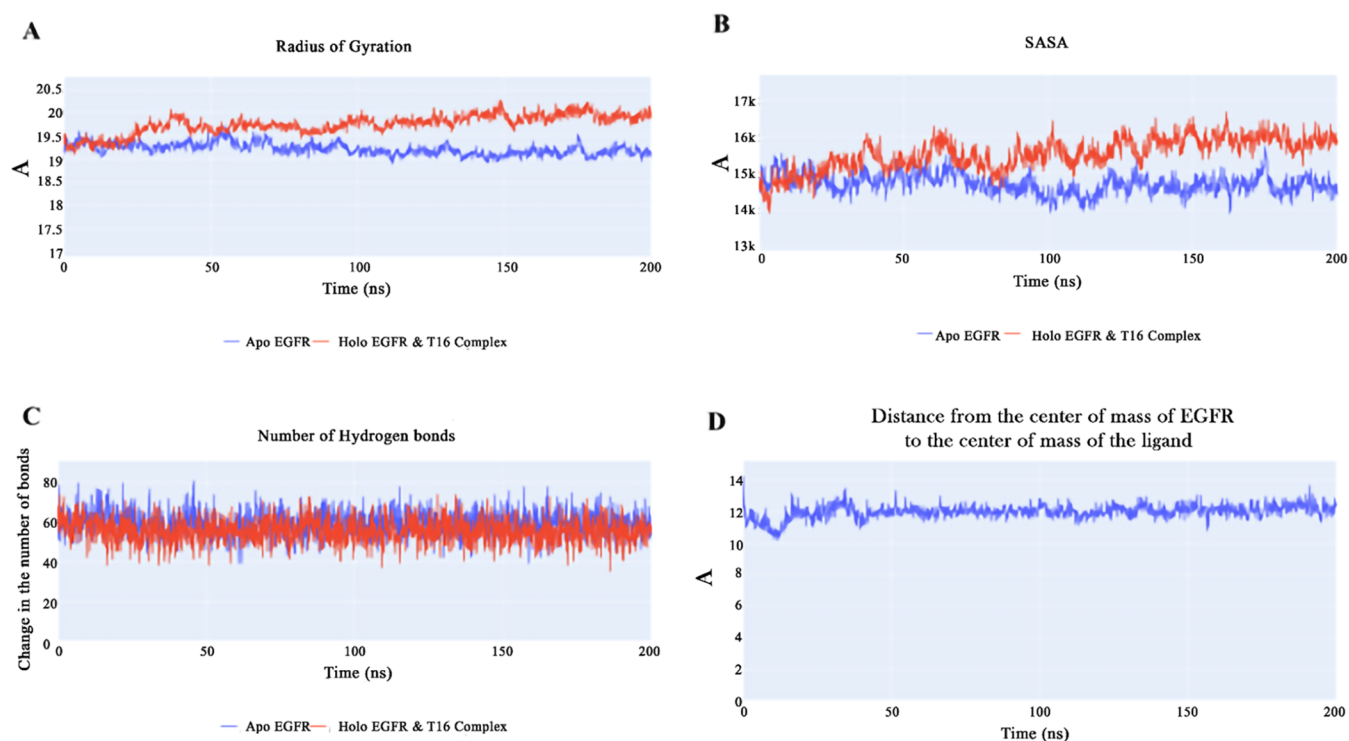


Figure 7. EGFR-T-1-PMPA complex dynamics: (A) EGFR protein's RG, (B) EGFR protein's SASA, (C) H.Bs average for the EGFR protein, and (D) T-1-PMPA and EGFR center of mass distances.

Different energy components of EGFR_T16 complex

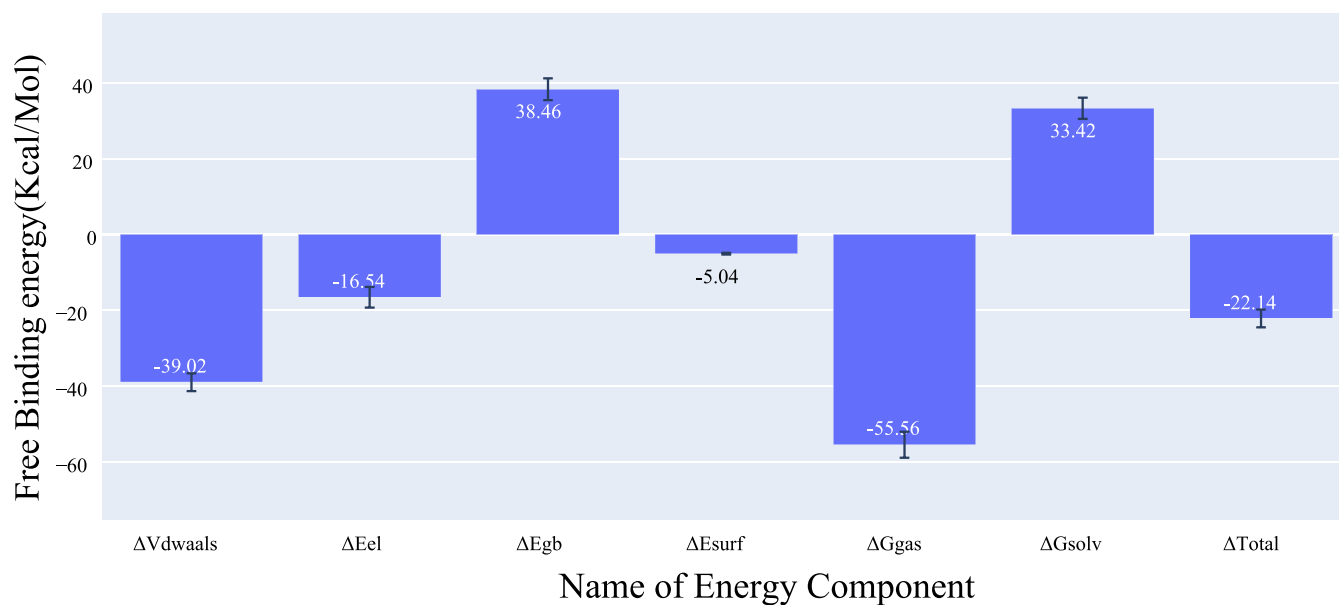


Figure 8. MM-GBSA energetic components and their values. Bars represent the standard deviations.

behavior and atomic-scale motions of molecular systems. These simulations involve numerically integrating atomic positions and velocities within a molecular system as it progresses through time. The foundational equations governing this integration process are derived from classical mechanics, primarily rooted in Newton's laws of motion.⁴⁹

Functioning as a potent tool, MD simulations provide extensive insights into diverse aspects of biomolecular behaviors. This encompasses understanding conformational

alterations, intermolecular interactions, and flexibility. MD simulations find wide application in various scientific domains, including structural biology, biochemistry, drug discovery, and materials science. Crucially, MD simulations complement experimental data, enriching our comprehension of intricate molecular processes such as biomolecular folding, protein–ligand interactions, and other significant biological phenomena.⁵⁰

MMGBSA free energy decomposition of residues within 1 nm of T16 in EGFR_T16 complex

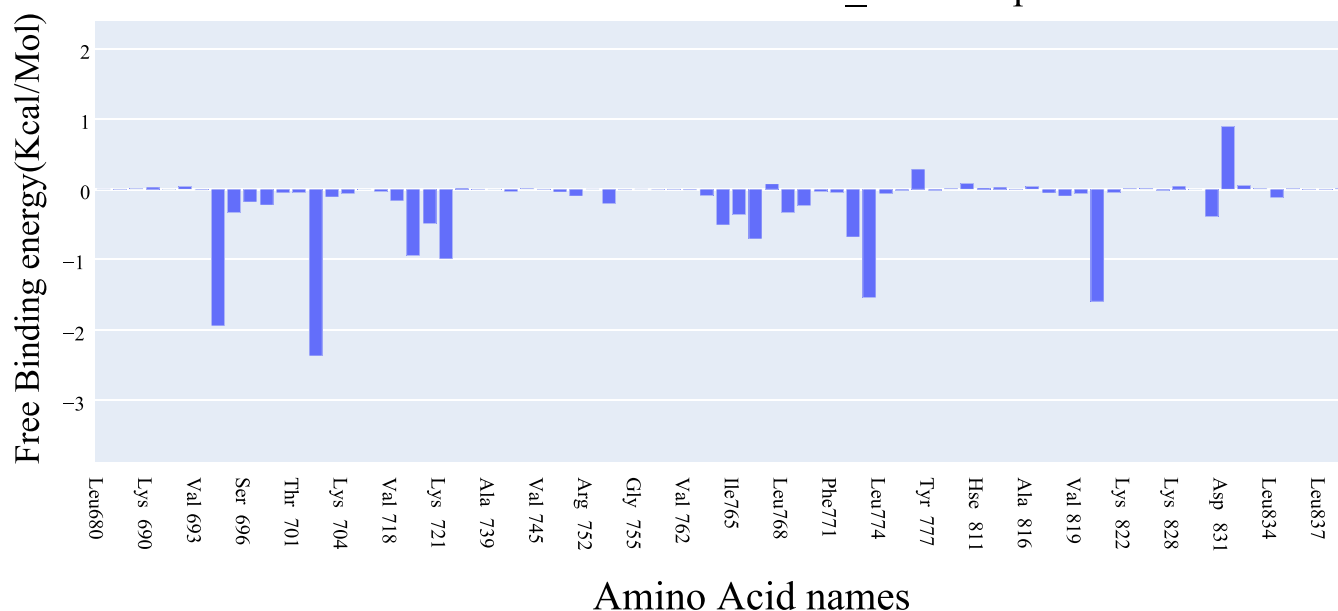


Figure 9. Decomposition of the EGFR_T1-PMMPA complex's binding free energy.

In this research, a 200 ns unbiased MD simulation in GROMACS 2021 was performed to assess the stability of the EGFR_T1-PMMPA complex and to investigate the structural changes between the apo EGFR and holo EGFR proteins.^{51,52} During the 200 ns production process, both the distance between T1-PMMPA and the EGFR's center of mass remained essentially consistent, as did the structure of the EGFR protein. After around 50 ns, the RMSD measurements for the apo EGFR protein (blue line) stabilized at about 2.3 Å. In contrast, the holo EGFR one displays an increasing trend for the first 37 ns before leveling off at an average of 2.6 Å (Figure 6A). After the first 50 ns, the RMSD of T1-PMMPA displays considerable oscillations around an average of 2.2 Å (Figure 6B), and then it was stabilized until the end of the experiment. The RMSF of the two systems exhibits essentially identical spikes, but there is a significant difference in the oscillations of C- α atoms in the Leu838:Val852 loop. It reaches a maximum of 5 Å for the holo EGFR protein and 3.6 Å for the apo EGFR system (Figure 6C).

Additionally, the radius of gyration (RG) for both the apo EGFR and holo EGFR systems diverges with time, as seen in Figure 7A. The holo EGFR system's RG values increased slightly (from 19.2 to 19.8 Å), whereas the apo EGFR system's RG values decreased slightly (from 19.3 to 19 Å). Similarly, the SASA for apo EGFR proteins decreases somewhat from 14,467 to 14,377 Å²; on the other hand, the SASA (Figure 7B) for holo EGFR proteins increases from 14,602 to 15,809 Å². This indicates that the apo EGFR protein is becoming somewhat more compact, while the holo EGFR protein is changing its shape, increasing its accessible surface area. Figure 7C shows that the average number of H.Bs in the apo EGFR system is somewhat higher (more compact) than in the holo EGFR system (59 bonds vs 55 bonds). Overall, this implies that each system is relatively stable, despite variances in their conformations. T1-PMMPA has a consistent average (about 12 Å) between the EGFR protein and T1-PMMPA centers of

mass, with modest changes suggesting a stable connection (Figure 7D).

2.1.6. MM-GBSA. The components of the binding free energy estimated using the MM-GBSA technique⁵³ are shown in Figure 8. The binding energy of T1-PMMPA is -22.14 kcal/mol, indicating a strong interaction. Van der Waals interactions (-39.02 kcal/mol) are more essential than electrostatic interactions (-16.54 kcal/mol) in determining the binding stability. The contributions of amino acids contained within 1 nm of T1-PMMPA were determined by using decomposition analysis (Figure 9). Less than -1 kcal/mol amino acids include Leu694 (-1.94 kcal/mol), Val702 (-2.37 kcal/mol), Cys773 (-1.54 kcal/mol), and Leu820 (-1.59 kcal/mol). Leu694, Gly695, Val702, Ala719, Lys721, Leu764, Thr766, Gly772, Cys773, Leu820, and Thr830 created very persistent hydrophobic interactions with T1-PMMPA (80% or more incidence).

2.1.7. Protein-Ligand Interaction Fingerprint (ProLIF) Study. ProLIF represents a vital technique employed within computer-aided drug design, molecular docking, and MD investigations. This method is instrumental in the comprehensive analysis and characterization of interactions between proteins and ligands. The ProLIF approach entails the generation of interaction fingerprints, a set of distinctive patterns arising from the interplay between a protein and a ligand. These fingerprints play a pivotal role in quantifying both the strength and nature of the binding interactions.⁵⁴ The ProLIF technique facilitates the quantification of various interaction types, encompassing critical categories such as hydrogen bonds, hydrophobic contacts, and other noncovalent associations. Furthermore, in the context of MD simulations, ProLIF serves as a valuable tool for monitoring the dynamic behavior of protein-ligand complexes over extended periods. It offers essential insights into the evolving interactions between the protein and the ligand throughout the simulation, thereby enhancing our understanding of complex stability and

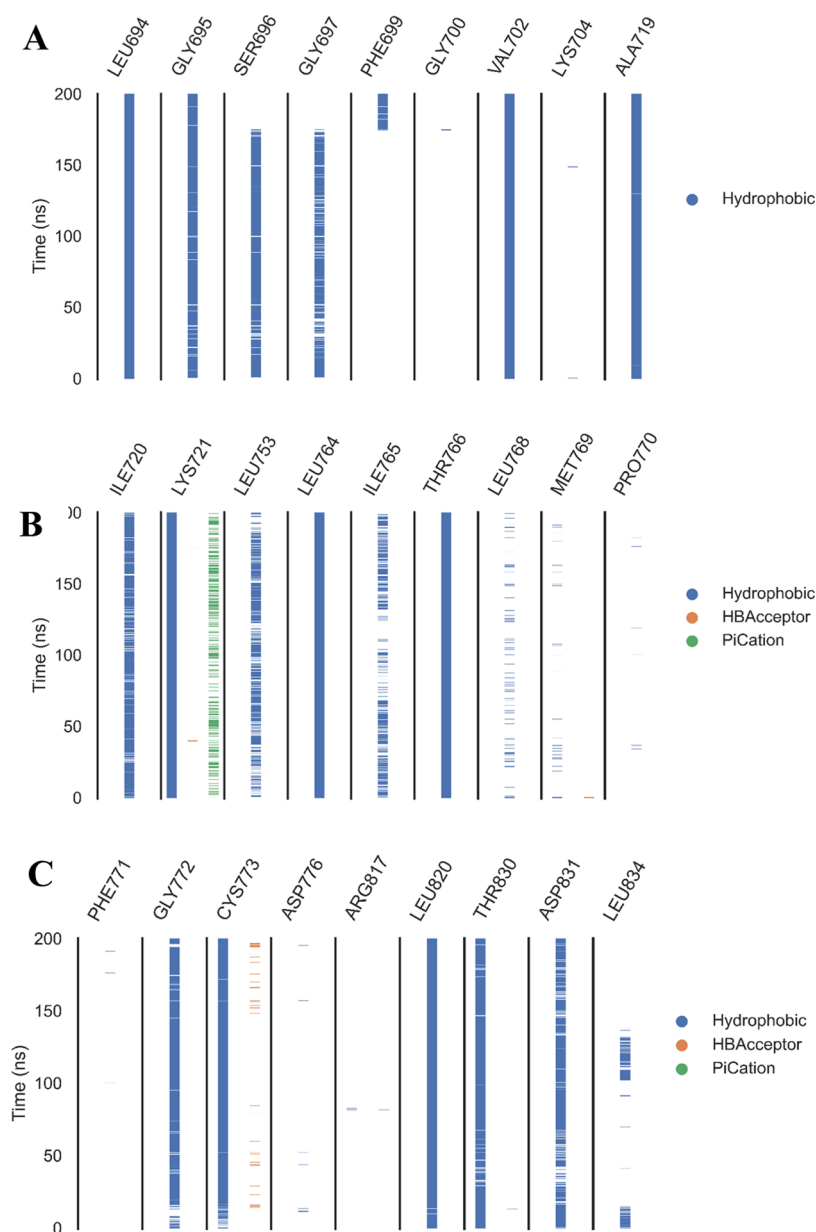


Figure 10. Interacting amino acids showing different residues (A–C) that reacted with T-1-PMPA during the 200 ns of the simulation.

binding affinity.⁵⁵ Using the ProLIF python library,⁵⁶ as shown in Figure 10, the amino acids Leu694, Gly695, Val702, Ala719, Lys721, Leu764, Thr766, Gly772, Cys773, Leu820, and Thr830 created very persistent hydrophobic interactions with T-1-PMPA (80% or more incidence) during the 200 ns of the simulation time.

2.1.8. Protein–Ligand Interaction Profiles (PLIP) Study. PLIP, an eminent bioinformatics approach, assumes an essential role in dissecting and depicting protein–ligand interactions. This computational tool offers crucial insights into the noncovalent connections as well as the binding interactions formed between the protein and the ligand. These discoveries elucidate the intricate molecular mechanisms that govern protein–ligand interactions.⁵⁷ PLIP, given its paramount importance across domains such as drug discovery, computational biology, and structural bioinformatics, has been widely adopted for the thorough examination of protein–ligand complexes and their interplay. Its incorporation with

other computational techniques, such as molecular docking, MD simulations, and free energy calculations, facilitates a deep understanding of interactions between ligands and proteins.⁵⁸ Consequently, PLIP stands as a pivotal method in the realm of rational drug design.⁵⁹

Subsequently, we subjected the trajectory data of the T-1-PMPA complex to a clustering procedure, yielding a solitary representative frame for each cluster formed. The number of clusters was automatically ascertained using the elbow method, ultimately giving rise to a sum of five discernible clusters.

Once the clusters were established, the next step was the selection of a representative frame from each cluster. These representative frames (Figure 11) served as exemplars or snapshots of the overall behavior exhibited in the 200 ns of the MD simulations and gave insights into the number and types of interactions occurring through the T-1-PMPA EGFR complex in each specific cluster.

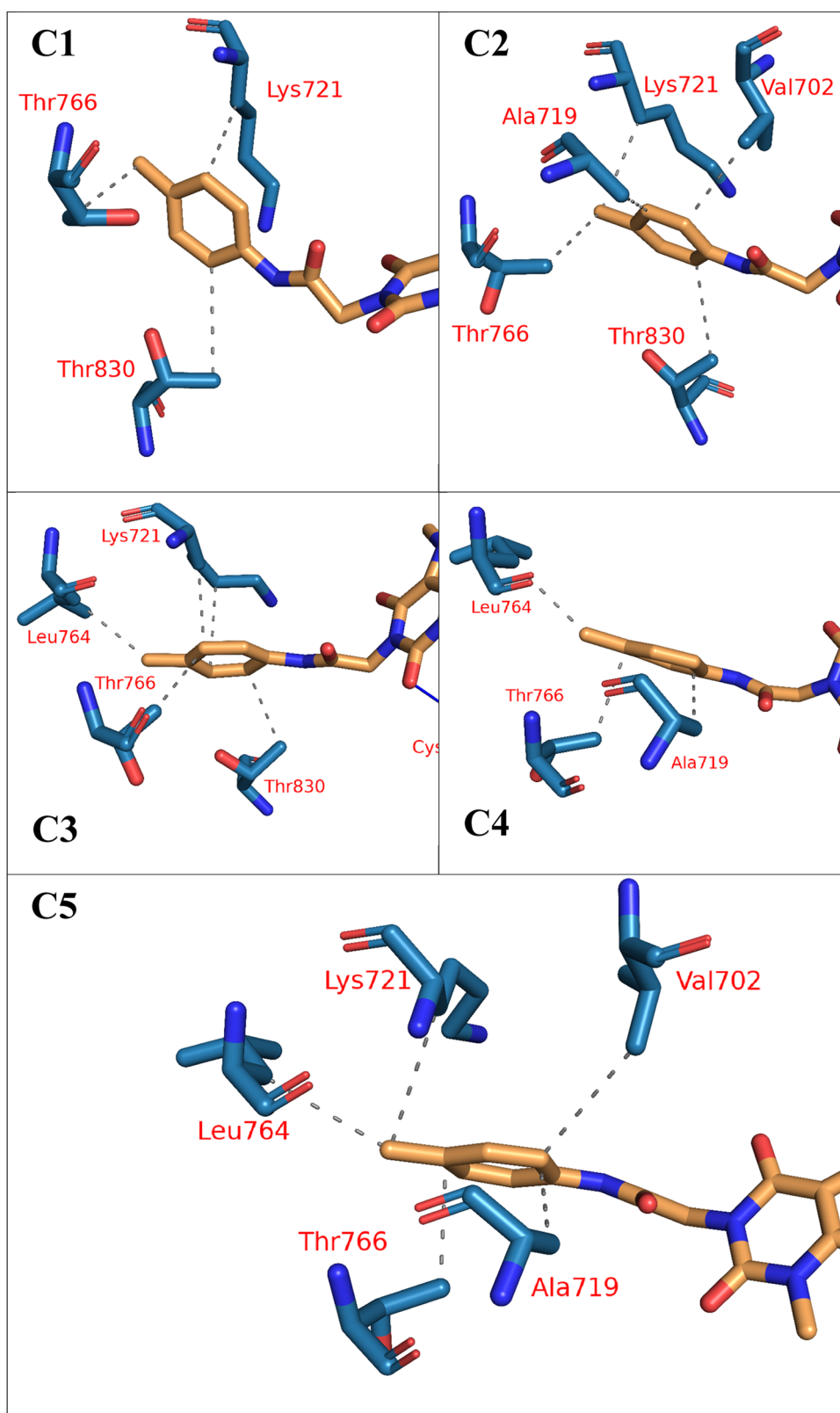


Figure 11. Five clusters (C1, C2, C3, C4, and C5) computed by the TTClust and their detailed interactions with T-1-PMPA. Gray dashed lines: H.I.s, blue solid lines: H.B.s, orange sticks: T-1-PMPA, blue sticks: amino acids of EGFR protein.

2.1.9. *Principal Component Analysis of Trajectories (PCAT) Studies.* PCAT, a well-established computational technique widely employed in the field of MD simulations, plays a pivotal role in the analysis of essential collective

motions from MD trajectory data. During the MD simulations, precise records of atomic positions within the examined complex are continuously logged over the time of experiment, resulting in a comprehensive trajectory that intricately captures

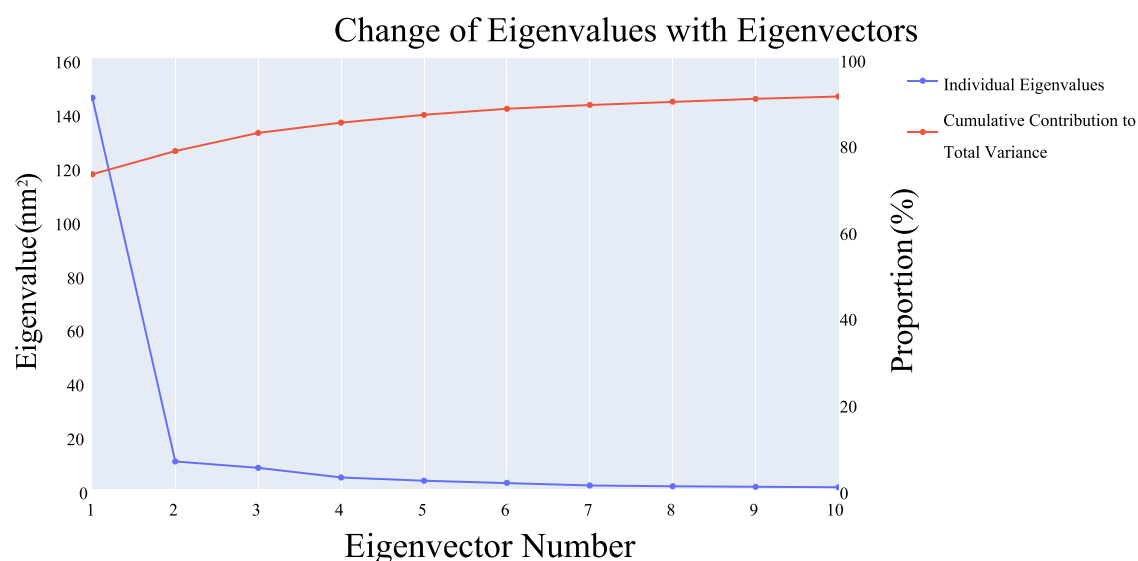


Figure 12. Eigenvalues change (blue line) when increasing eigenvectors, and the cumulative variance retained in them (red line).

Histogram of the first 10 PCs

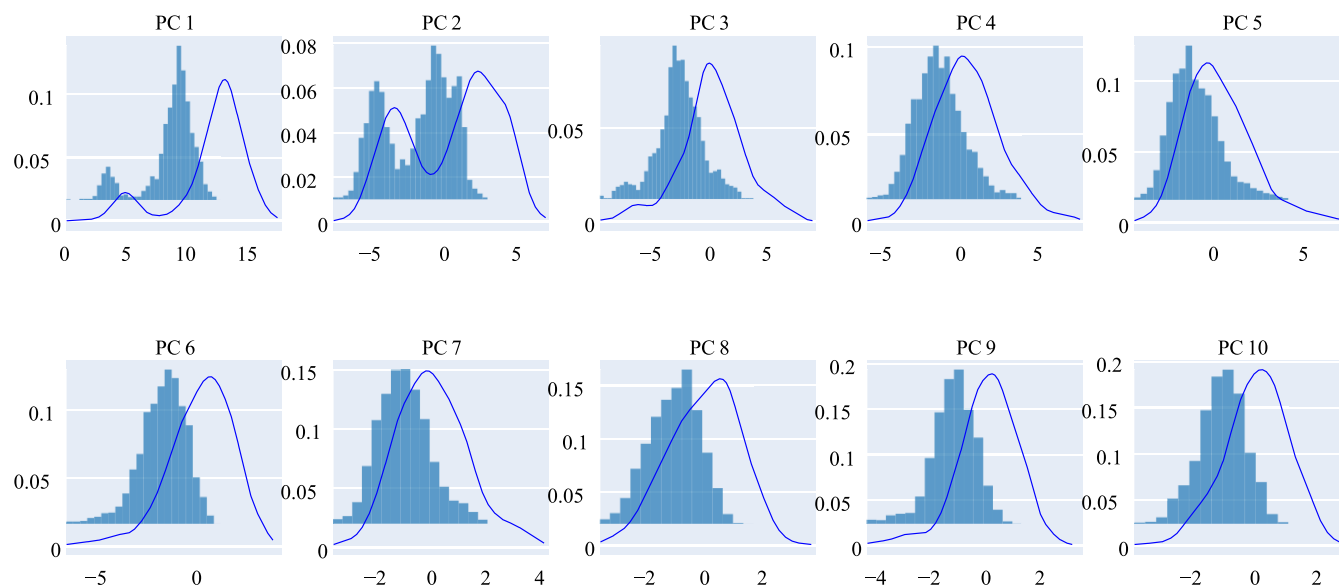


Figure 13. First ten eigenvectors' distribution.

the dynamic behavior of the system.⁶⁰ At this juncture, PCAT's intervention becomes indispensable as it simplifies this intricate trajectory. This simplification is achieved by Mapping the trajectory onto a space with fewer dimensions while preserving the most critical motions. After this simplification, PCAT effectively highlights the dominant motions governing the system's functionality and behavior, providing deep insights into the fundamental collective motions that underlie the biomolecular dynamics of the system. The coordinated motion was discovered using principal component analysis (PCA).^{61,62}

In this study, we employed the scree plot, eigenvector distribution, and cumulative sum of retained variance with additional eigenvectors to determine the dimensionality of the reduced subspace. The scree plot revealed a notable change in the slope at the second principal component (PC). The initial eigenvector singularly explained 73.1% of the overall variance,

while the cumulative contribution of the first three eigenvectors accounted for approximately 82% of the total variance (Figure 12). The distribution of the first three PCs was shown to be non-Gaussian (Figure 13). Therefore, we opted for the utilization of the top three eigenvectors in order to represent the reduced subspace.

2.1.9.1. Cosine Content Calculations. The cosine content was calculated for both apo EGFR and holo EGFR simulations in order to evaluate the randomness of the first 10 eigenvectors' behavior.⁶³ The cosine content of the initial ten eigenvectors is less than 0.25 in both the apo EGFR and holo EGFR proteins (Figure 14). The low overlap between the first three eigenvectors in the two subspaces showing 19.4% according to the Root Mean Square Inner Product (RMSIP) indicates that the two trajectories sampled in a different way. Additionally, the RMSIP investigation revealed that the C

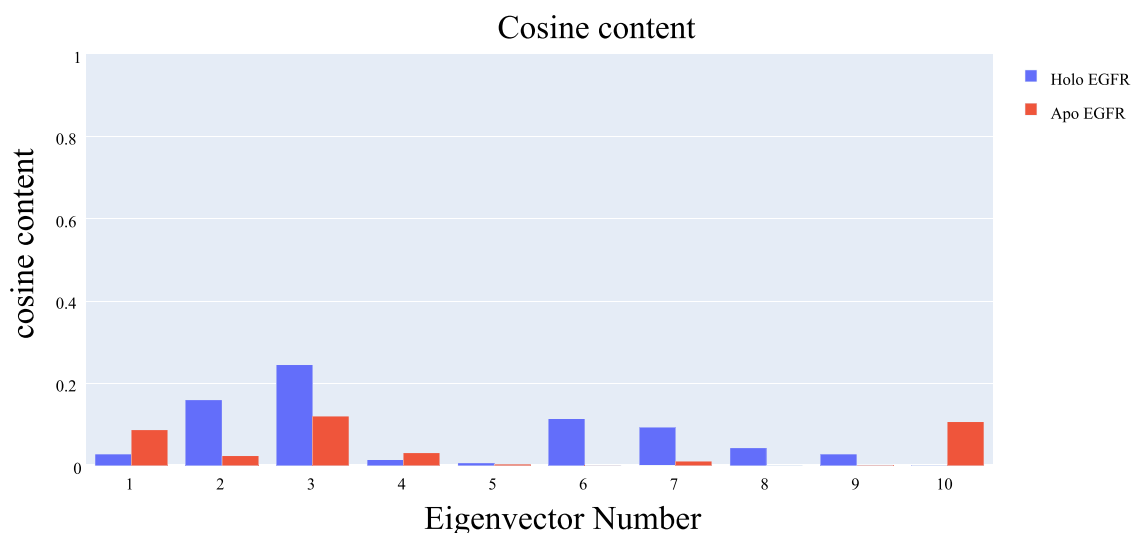


Figure 14. Cosine content's values of the first ten eigenvectors for the two (apo EGFR and holo EGFR) trajectories.

matrices of apo EGFR and holo EGFR proteins were similar in a ratio of 32.9%.

2.1.9.2. Bidimensional Projection Analysis. The outcomes of projecting individual trajectories onto the three initial eigenvectors of the entire C matrix are illustrated in Figure 15. Each graph portrays the average structure of each trajectory, with the larger dot representing this average. In Figure 15A (depicting a projection on the first two eigenvectors), two distinctive average structures for the two trajectories are evident, with only a brief overlap at the simulation's outset (pale red and white dots). Figure 15B demonstrates a significant overlap between the two trajectories, indicating comparable average structures. The projection onto the second and third eigenvectors (Figure 15C) reveals that the two trajectories are distinct, with minimal overlap observed only in the initial frame.

Visual representations of molecular dynamics simulations play a pivotal role in gaining insight into the dynamic behaviors of biological molecules. In our study, we employed porcupine figures as a visual tool to portray the motion patterns observed in the first three eigenvectors for both the holo and apo systems of the EGFR-T-1-PMPA complex. Specifically, we utilized green cartoon representations to depict the trajectory of the apo EGFR protein and red cartoon representations for the holo EGFR protein. These porcupine figures essentially serve as dynamic snapshots, capturing the fluctuations and movements of the molecules throughout the simulation. Each eigenvector corresponds to a unique mode of motion, and these figures assist us in understanding how these modes contribute to the overall behavior of the proteins. Porcupine diagrams of the first three eigenvectors (Figure 16) show that in the first and second PCs, the apo EGFR protein (red structure) displays a closure of the Phy832:Pro853 loop, but the holo EGFR protein (green structure) displays an opening. This is consistent with decreasing/increasing RoG and SASA values for each structure. On the other hand, the third PC demonstrates the opposite for the holo EGFR protein (loop opening), while the apo EGFR protein does not exhibit substantial movements.

2.2. Semisynthesis. The semisynthetic route to produce T-1-PMPA is shown in Scheme 1. According to the reported procedures, the potassium salt, 2, was made by refluxing

theobromine 1 with KOH in absolute ethanol.⁶⁴ Dropping chloroacetyl chloride into a stirred mixture of *p*-toluidine, 3, in DMF in an ice salt bath afforded the key intermediate, 2-chloro-*N*-(*p*-tolyl)acetamide 4 in a good yield (85%). T-1-PMPA was prepared by refluxing a 1:1 mixture of compounds 2 and 4 in a DMF/KI mixture. The chemical structure of T-1-PMPA was confirmed through EI-MS, elemental analysis, and ¹H and ¹³C NMR spectroscopy (details in the method part and in the Supporting Information).

2.3. In Vitro Biological Assessments. **2.3.1. Multikinase Inhibition.** In order to assess the effectiveness of the designed compound, T-1-PMPA, against the EGFR^{WT} protein, an *in vitro* investigation was conducted. This analysis aimed to evaluate the alignment between the computational results and the experimental outcomes, thus validating the potential of the compound. T-1-PMPA exhibited a significant inhibition against the EGFR^{WT} and EGFR^{T90M} proteins, with IC₅₀ values of 86 and 561.73 nM, respectively (Table 6). These findings corroborated the *in silico* predictions, reinforcing T-1-PMPA's promising suppressive capabilities. Regarding VEGFR-2, T-1-PMPA exhibited a low degree of inhibition with an IC₅₀ value of 2.07 μM compared to sorafenib (0.35 μM).

2.3.2. In Vitro Cytotoxicity and Safety. Given the remarkable inhibitory potential demonstrated by T-1-PMPA against EGFR^{WT}, both *in silico* and *in vitro*, it holds great promise as an effective agent in cancer treatment. To further evaluate its cytotoxicity, T-1-PMPA was tested *in vitro* against two cancer cell lines: HepG2 and MCF7. Erlotinib was used as a reference drug for comparison (Table 7). Interestingly, T-1-PMPA exhibited significant anticancer activity against both cell lines, with IC₅₀ values of 3.51 ± 0.02 and 4.13 ± 0.08 μM, respectively, whereas Erlotinib displayed IC₅₀ values of 2.24 ± 0.06 and 3.17 ± 0.01 μM, respectively. To assess the safety and specificity of T-1-PMPA, experiments were conducted by using the Vero cell line. Results indicated that T-1-PMPA exhibited a substantial IC₅₀ value of 196.4 μM and displayed remarkably high selectivity indexes (SI) of 56 and 48 against the two cancer cell lines, respectively.

2.3.3. Apoptosis Detection. **2.3.3.1. Flow Cytometry Assay.** Apoptosis, a programmed cell death process, plays a vital role in maintaining a balance between cell production and cell death, thus ensuring homeostatic equilibrium. However,

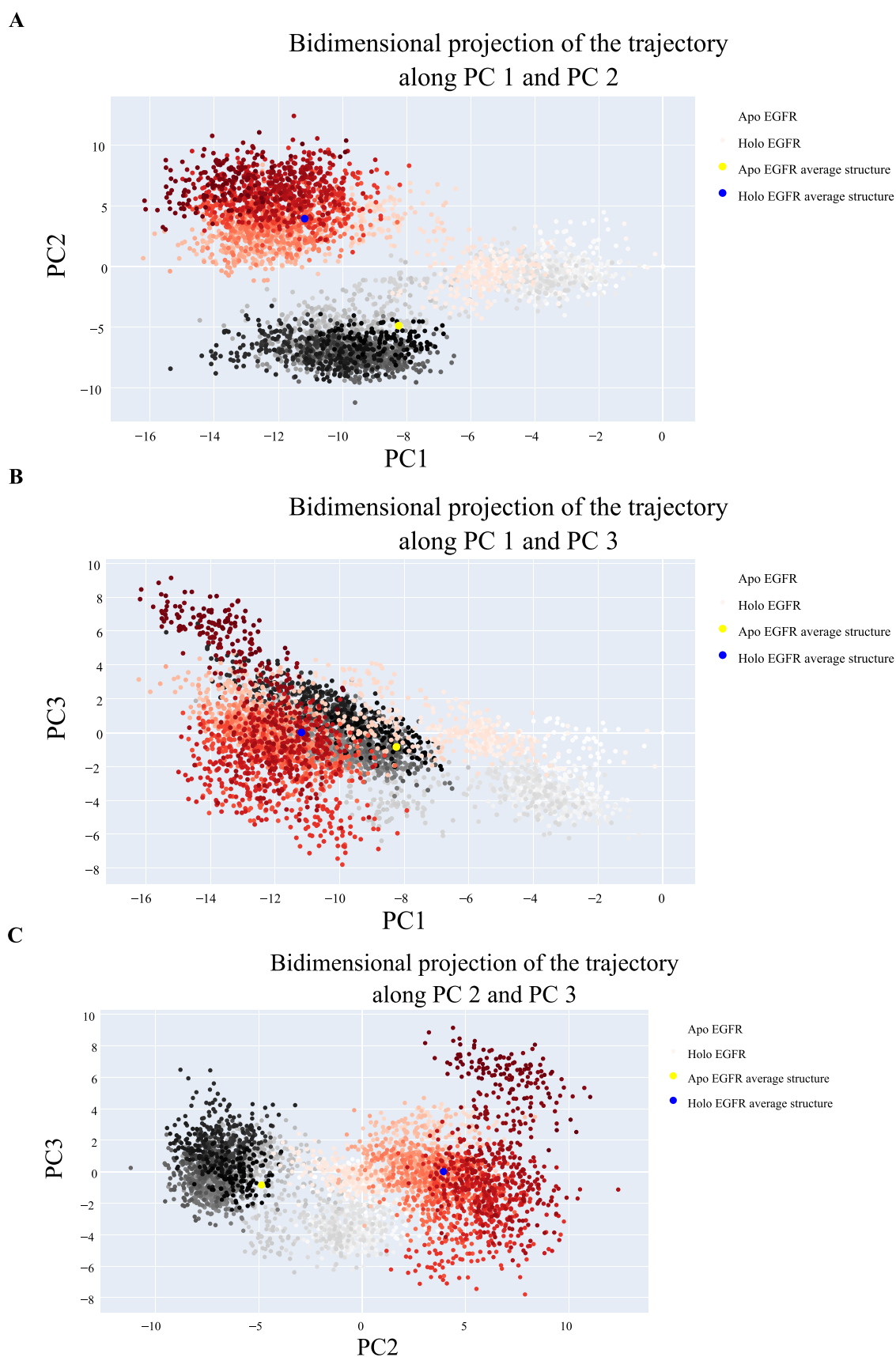


Figure 15. Projection of each trajectory on (A) first two, (B) first and third, and (C) second and third eigenvectors.

disruptions in this balance can contribute to abnormal cell development, excessive cell proliferation, autoimmune diseases,

and more. Throughout the development of an embryo and the growth of an organism, apoptosis is considered crucial for

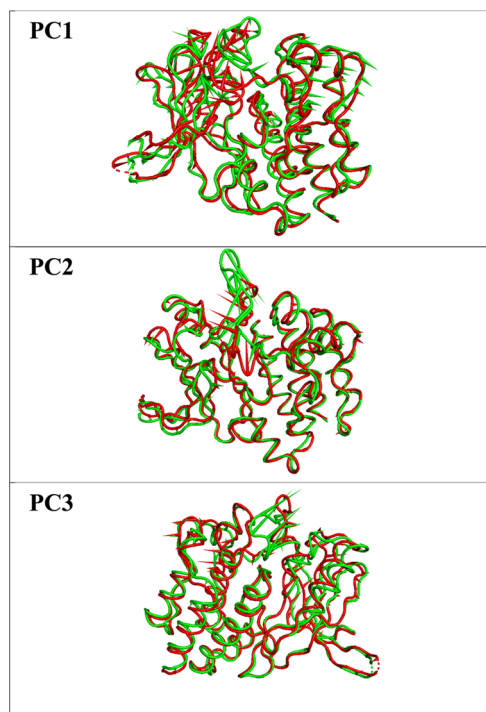


Figure 16. Porcupine figures of each of the first three eigenvectors (PC1, PC2, and PC3) for holo EGFR protein (green cartoon) trajectory and apo EGFR protein (red cartoon) trajectory.

tissue regeneration and the elimination of inflammatory cells, thereby supporting overall health and function.⁶⁵ In the 1980s, the observation of DNA breakage in thymocytes exposed to glucocorticoids led to the recognition of apoptosis induction as a logical and viable therapeutic approach.^{4,66}

To validate the apoptotic properties of T-1-PMPA, the percentage of apoptotic cells in HepG2 cells was assessed using Annexin V and PI double stains.⁶⁷ The findings demonstrated that T-1-PMPA increased the proportion of cells in the early stage of apoptosis from 0.77 to 29.17%, the late stage of apoptosis from 0.17 to 8.81%, and the overall stage from 3.05 to 42.03%. Additionally, the percentage of necrotic cells increased to 4.05% compared to 2.21% in the control cells (Figure 17 and Table 8). Interestingly, T-1-PMPA's results

Scheme 1. Semisynthesis of T-1-PMPA

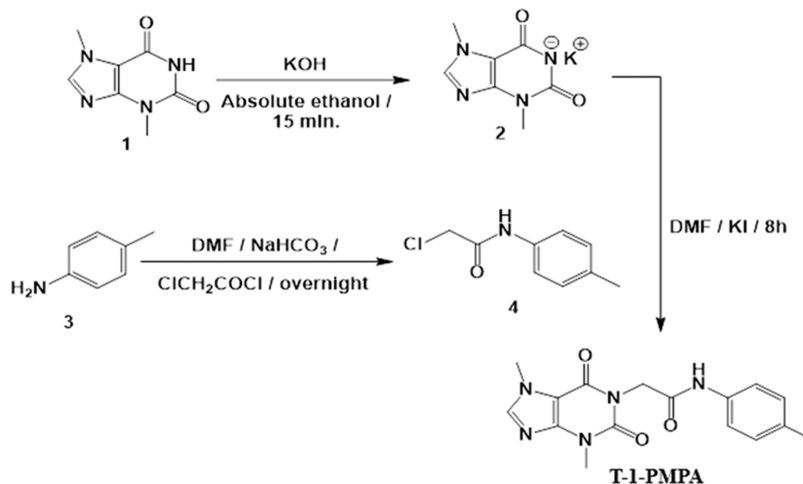


Table 6. IC₅₀ Values of T-1-PMPA and Erlotinib against EGFR^{WT} and EGFR^{790m} Kinases

| comp. | EGFR ^{WT} IC ₅₀ (nM) | EGFR ^{790m} IC ₅₀ (nM) |
|-----------|--|--|
| T-1-PMPA | 86 | 561.73 |
| Erlotinib | 31 | 455.86 |

Table 7. *In Vitro* Antiproliferative T-1-PMPA against HepG2 and MCF7 Cell Lines

| comp. | <i>in vitro</i> cytotoxicity IC ₅₀ (μM) ^a | |
|-----------|---|-------------|
| | HepG2 | MCF7 |
| T-1-PMPA | 3.51 ± 0.02 | 4.13 ± 0.08 |
| Erlotinib | 2.24 ± 0.06 | 3.17 ± 0.01 |

^aData are presented as three times the mean values of IC₅₀.

were stronger than those of Erlotinib in total and early stages, while it was a little bit weaker in the late stage.

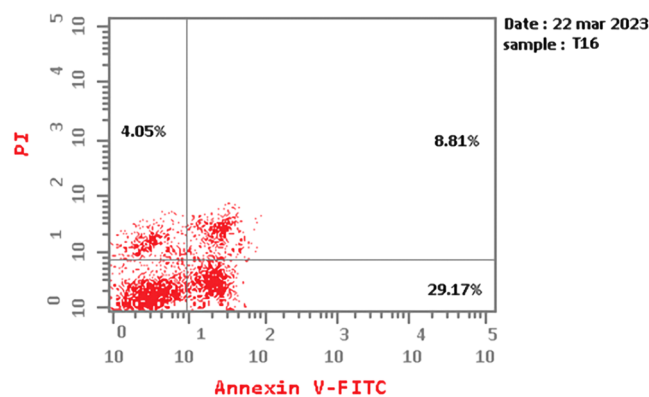


Figure 17. Flow cytometric charts of apoptosis in HepG2 cells exposed to T-1-PMPA.

2.3.3.2. qRT-PCR Assay. This study focused on investigating the effects of T-1-PMPA on HepG2 cells, specifically examining the expression levels of caspase-3 and caspase-9 proteins. T-1-PMPA was administered at a concentration of 3.51 μM, corresponding to its IC₅₀ value. The results revealed significant alterations in the expression levels of these proteins compared with the control group. Notably, the study

Table 8. Effects of T-1-PMPA and Erlotinib on the Stages of the Cell Death Process in HepG2 Cells

| comp. | apoptosis | | | necrosis |
|---------------------|-----------|-------|------|----------|
| | total | early | late | |
| T-1-PMPA | 42.03 | 29.17 | 8.81 | 4.05 |
| Erlotinib | 31.19 | 18.73 | 9.44 | 3.02 |
| control HepG2 cells | 3.05 | 0.77 | 0.17 | 2.21 |

demonstrated a significant elevation in the levels of caspase-3 and caspase-9 upon T-1-PMPA treatment. Caspases make up a family of enzymes that play a crucial role in the apoptotic process. Caspase-3 serves as an initiator caspase, activated at the initial stages of the apoptotic pathway,⁶⁸ while caspase-9 functions as an executioner caspase, activated downstream in the pathway.⁶⁹ The observed 5.97-fold increase in caspase-3 level and 4.57-fold increase in caspase-9 level relative to the control indicate that T-1-PMPA acts as a promoter of apoptosis. Interestingly, as shown in Table 9, the observed

Table 9. T-1-PMPA's Activities on Apoptotic Proteins in HepG2 Cell Lines

| sample | RT-PCR (fold change) | |
|-----------|----------------------|-------|
| | Casp3 | Casp9 |
| T-1-PMPA | 5.97 | 4.57 |
| Erlotinib | 6.87 | 6.02 |
| control | 1 | 1 |

results were near to those of Erlotinib that exhibited 6.87-fold increase in caspase-3 level and 6.02-fold increase in caspase-9 level relative to the control. These findings provide valuable insights into the mechanism of action of T-1-PMPA and its potential as an anticancer agent.

2.3.4. Inhibition of Inflammatory Mediators. The role of chronic inflammation in the development and progression of different cancer types has been widely acknowledged.⁷⁰ Inflammatory mediators, including cytokines and chemokines, have been implicated in promoting cancer cell growth, survival, and metastasis. These mediators induce angiogenesis, suppress immune surveillance, and cause genetic instability and DNA damage. Also, inflammatory mediators have been found to upregulate the expression of kinases through complex mechanisms involving multiple intracellular signaling pathways that synergistically enhance kinase expression and its pro-angiogenic functions.⁷¹ Moreover, several studies have demonstrated the connection between EGFR expression and the production of proinflammatory cytokines, such as interleukins (ILs)^{72,73} and tumor necrosis factor- α (TNF- α), in various cell types.⁷⁴

To investigate further, the levels of TNF- α and IL2 were assessed in both the treated and control cancer cells. Interestingly, T-1-PMPA displayed a reduction in the production of proinflammatory cytokines TNF- α and IL2 by 74, and 49%, respectively, comparing to Erlotinib that expressed a reduction by 84 and 74%, respectively (Table 10). These findings suggest an additional antiangiogenic mechanism employed by T-1-PMPA, highlighting its potential in countering inflammatory processes.

3. EXPERIMENTAL SECTION

3.1. Docking Studies. Docking studies were operated for T-1-PMPA against EGFR^{WT} (wild form) and EGFR^{T790M}

Table 10. Inhibition of T-1-PMPA against TNF- α and IL2

| sample | RT-PCR (fold change) | |
|-----------------|----------------------|-------|
| | TNF α | IL2 |
| T-1-PMPA | 0.262 | 0.502 |
| Erlotinib | 0.158 | 0.261 |
| untreated cells | 1 | 1 |

(mutant form) by MOE2014 software.⁷⁵ The Supporting Section of this document offers detailed representations and additional elaborations.

3.2. MD Simulations. The simulation studies were operated for the EGFR-T-1-PMPA complex by the CHARMM-GUI web server and GROMACS 2021.⁷⁶ The Supporting Section of this document offers detailed representations and additional elaborations.

3.3. MM-GBSA. These studies were operated for the EGFR-T-1-PMPA complex by the Gmx_MMPBSA package.⁷⁷ The Supporting Section of this document offers detailed representations and additional elaborations.

3.4. ED Analysis. PCA was employed for the EGFR-T-1-PMPA complex to investigate the dynamic motion of α carbons located in the amino acid sequence spanning from Glu826 to Leu1161.⁷⁸ The Supporting Section of this document offers detailed representations and additional elaborations.

3.5. Bidimensional Assays. To compare frames within the reduced subspace, we merged, aligned, created a new C matrix, and plotted the projections.⁶⁰ The Supporting Section of this document offers detailed representations and additional elaborations.

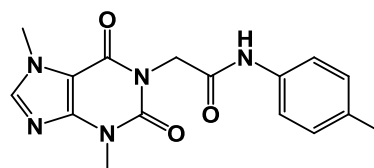
3.6. DFT. The DFT studies were operated for T-1-PMPA by Gaussian 09 and GaussSum3.0 programs. The Supporting Section of this document offers detailed representations and additional elaborations.

3.7. ADMET Studies. The ADMET studies were operated computationally for T-1-PMPA by Discovery Studio 4.0.⁷⁹ The Supporting Section of this document offers detailed representations and additional elaborations.

3.8. Toxicity Studies. The toxicity studies were operated computationally for T-1-PMPA by Discovery Studio 4.0.⁸⁰ The Supporting Section of this document offers detailed representations and additional elaborations.

3.9. Semisynthesis of T-1-PMPA. A solution (0.001 mol) of 2-Chloro-N-(p-tolyl)acetamide 4 was introduced to a solution of potassium 3,7-dimethyl-3,7-dihydro-1H-purine-2,6-dione 2 (0.001 mol) in dry DMF (10 mL). The mixture underwent heating in a water bath for 8 h. Following this, the reaction mixture was poured onto ice water (200 mL) and gently stirred for a specified duration. The resulting precipitate, corresponding to T-1-PMPA, was isolated through filtration, washed with water, and subjected to crystallization using methanol.

3.9.1. 2-(3,7-Dimethyl-2,6-dioxo-2,3,6,7-tetrahydro-1H-purin-1-yl)-N-(p-tolyl)acetamide. White powder (yield,



86%); mp = 207–209 °C; ¹H NMR (400 MHz, DMSO-*d*₆) δ 10.13 (s, 1H, NH), 8.08 (s, 1H, CH imidazole), 7.44 (d, *J* = 8 Hz, 2H, Ar–H), 7.11 (d, *J* = 8 Hz, 2H, Ar–H), 4.65 (s, 2H, CH₂), 3.90 (s, 3H, CH₃), 3.45 (s, 3H), 2.25 (s, 3H, CH₃); ¹³C NMR (101 MHz, DMSO-*d*₆) δ 165.89, 154.67, 151.38, 148.96, 143.68, 136.73, 132.70, 129.62 (2C), 119.50 (2C), 107.07, 43.78, 33.66, 29.91, 20.88; Mass (*m/z*): 327 (M⁺, 35%), 236 (100%, base peak); Anal. Calcd for C₁₆H₁₇N₅O₃ (327.34): C, 58.71; H, 5.23; N, 21.39; Found: C, 58.92; H, 5.40; N, 21.57%.

3.10. In Vitro EGFR Inhibition. The *in vitro* EGFR inhibition assays were operated for T-1-PMPA against EGFR^{WT} (wild form) and EGFR^{T790M} (mutant form) using Human EGFR ELISA kits. The Supporting Information shows a comprehensive explanation.

3.11. In Vitro Antiproliferative Activity. The *in vitro* antiproliferative activity was operated for T-1-PMPA by MTT procedure.^{81,82} The Supporting Information shows a comprehensive explanation.

3.12. Safety Assay. The safety profile of T-1-PMPA was examined *in vitro* by the calculation of the selectivity index after an MTT assay utilizing Vero cell lines.⁸³ The Supporting Section of this document offers detailed representations and additional elaborations.

3.13. Flow Cytometry of Apoptosis. This assay was operated for T-1-PMPA using the flow cytometry analysis technique. The Supporting Section of this document offers detailed representations and additional elaborations.

3.14. Apoptotic Proteins Assay. Apoptotic proteins assay was operated by RT-PCR using the Qiagen RNA extraction/BioRad syber green PCR MMX kit. The Supporting Section of this document offers detailed representations and additional elaborations.

4. CONCLUSIONS

In conclusion, utilizing the essential structural characteristics of existing EGFR inhibitors, we successfully developed a new apoptotic semisynthetic derivative (T-1-PMPA) starting from the natural alkaloid theobromine. DFT computations validated the 3D structure of T-1-PMPA and indicated its high reactivity. Through molecular docking and 200 ns MD simulations, we confirmed T-1-PMPA's binding affinity and inhibitory potential against EGFR, further supported by *in vitro* experiments. *In vitro* studies demonstrated that T-1-PMPA effectively inhibited EGFR^{WT}. Moreover, T-1-PMPA exhibited significant suppression of proliferation in HepG2 and MCF7 malignant cell lines, with favorable selectivity indices indicating its overall safety. Importantly, T-1-PMPA induced apoptosis, as evidenced by the increase in the total percentage of apoptotic cells compared to the control. Furthermore, qRT-PCR analysis revealed significant upregulation of Casp3 and Casp9, further confirming the apoptotic effects of T-1-PMPA. These findings highlight the potential of T-1-PMPA as a promising EGFR inhibitor with apoptotic properties. The successful design and evaluation of T-1-PMPA provide insights into the development of targeted therapies against EGFR-overexpressing carcinomas, opening avenues for further chemical modifications and potential clinical applications.

■ ASSOCIATED CONTENT

Data Availability Statement

The manuscript and Supporting Materials encompass all of the data related to this research.

SI Supporting Information

The Supporting Information is available free of charge at <https://pubs.acs.org/doi/10.1021/acsomega.3c08148>.

¹H NMR, ¹³C NMR, EI-Ms spectra for T-1-PMPA, and additional information on experimental details, materials, and methods, including photographs of the experimental setup; and the QTAIM parameters at bond critical points (BCPs) in addition to the toxicity report of T-1-PMPA were also included (PDF)

■ AUTHOR INFORMATION

Corresponding Authors

Hazem Elkady – Pharmaceutical Medicinal Chemistry & Drug Design Department, Faculty of Pharmacy (Boys), Al-Azhar University, Cairo 11884, Egypt; Email: hazemelkady@azhar.edu.eg

Ahmed M. Metwaly – Pharmacognosy and Medicinal Plants Department, Faculty of Pharmacy (Boys), Al-Azhar University, Cairo 11884, Egypt; Biopharmaceutical Products Research Department, Genetic Engineering and Biotechnology Research Institute, City of Scientific Research and Technological Applications (SRTA-City), Alexandria 21934, Egypt; orcid.org/0000-0001-8566-1980; Email: ametwaly@azhar.edu.eg

Authors

Ibrahim H. Eissa – Pharmaceutical Medicinal Chemistry & Drug Design Department, Faculty of Pharmacy (Boys), Al-Azhar University, Cairo 11884, Egypt; orcid.org/0000-0002-6955-2263

Reda G. Yousef – Pharmaceutical Medicinal Chemistry & Drug Design Department, Faculty of Pharmacy (Boys), Al-Azhar University, Cairo 11884, Egypt

Eslam B. Elkaeed – Department of Pharmaceutical Sciences, College of Pharmacy, AlMaarefa University, Riyadh 13713, Saudi Arabia

Aisha A. Alsfolk – Department of Pharmaceutical Sciences, College of Pharmacy, Princess Nourah bint Abdulrahman University, Riyadh 11671, Saudi Arabia; orcid.org/0000-0003-4497-5013

Dalal Z. Husein – Chemistry Department, Faculty of Science, New Valley University, El-Kharja 72511, Egypt

Ibrahim M. Ibrahim – Biophysics Department, Faculty of Science, Cairo University, Giza 12613, Egypt

Ahmed Ismail – Biochemistry and Molecular Biology Department, Faculty of Pharmacy, Al-Azhar University, Cairo 11884, Egypt

Complete contact information is available at: <https://pubs.acs.org/10.1021/acsomega.3c08148>

Author Contributions

The study was conceptualized and designed by I.H.E. and A.M.M. A.M.M., H.E., and E.B.K. supervised the work. The semisynthesis was performed by R.G.Y. and H.E., while D.Z.H., H.E., and I.M.I. conducted the computational studies. Biological investigations were carried out by A.I. The funding for the study was obtained by E.B.E. and A.A.A., who also contributed to writing the manuscript. All authors have thoroughly reviewed and approved the final manuscript, taking responsibility for its scientific validity, originality, and ensuring it meets the required standards for the similarity index.

Funding

This research was funded by the Princess Nourah bint Abdulrahman University Researchers Supporting Project number PNURSP2024R116, Princess Nourah bint Abdulrahman University, Riyadh, Saudi Arabia.

Notes

The authors declare no competing financial interest.

Ethical Approval Statement There is no ethical issue regarding this work.

Sample Availability T-1-PMPA is available from the authors.

ACKNOWLEDGMENTS

The authors express sincere gratitude to AlMaarefa University, Riyadh, Saudi Arabia, for supporting this research.

REFERENCES

- (1) Siegel, R. L.; Miller, K. D.; Fuchs, H. E.; Jemal, A. Cancer statistics, 2022. *Ca-Cancer J. Clin.* **2022**, *72* (1), 7–33.
- (2) Khan, F.; Akhtar, S.; Kamal, M. A. Nanoinformatics and Personalized Medicine: An Advanced Cumulative Approach for Cancer Management. *Curr. Med. Chem.* **2023**, *30* (3), 271–285.
- (3) Voss, A. K.; Strasser, A. The essentials of developmental apoptosis. *F1000Research* **2020**, *9*, No. 148.
- (4) Carneiro, B. A.; El-Deiry, W. S. Targeting apoptosis in cancer therapy. *Nat. Rev. Clin. Oncol.* **2020**, *17* (7), 395–417.
- (5) Goel, S.; Hidalgo, M.; Perez-Soler, R. EGFR inhibitor-mediated apoptosis in solid tumors. *J. Exp. Ther. Oncol.* **2007**, *6* (4), 305–320.
- (6) Gong, Y.; Somwar, R.; Politi, K.; Balak, M.; Chmielecki, J.; Jiang, X.; Pao, W. Induction of BIM is essential for apoptosis triggered by EGFR kinase inhibitors in mutant EGFR-dependent lung adenocarcinomas. *PLoS Med.* **2007**, *4* (10), No. e294.
- (7) Rosenkranz, A. A.; Slastnikova, T. A. Epidermal Growth Factor Receptor: Key to Selective Intracellular Delivery. *Biochemistry (Moscow)* **2020**, *85* (9), 967–1092.
- (8) Kaufman, N. E. M.; Dhingra, S.; Jois, S. D.; Vicente, M. Molecular Targeting of Epidermal Growth Factor Receptor (EGFR) and Vascular Endothelial Growth Factor Receptor (VEGFR). *Molecules* **2021**, *26* (4), No. 1076, DOI: 10.3390/molecules26041076.
- (9) Normanno, N.; Bianco, C.; De Luca, A.; Salomon, D. S. The role of EGF-related peptides in tumor growth. *Front. Biosci.* **2001**, *6* (3), 685–707.
- (10) Spano, J. P.; Lagorce, C.; Atlan, D.; Milano, G.; Domont, J.; Benamouzig, R.; Attar, A.; Benichou, J.; Martin, A.; Morere, J. F.; Raphael, M.; Penault-Llorca, F.; Breau, J. L.; Fagard, R.; Khayat, D.; Wind, P. Impact of EGFR expression on colorectal cancer patient prognosis and survival. *Ann. Oncol.* **2005**, *16* (1), 102–108.
- (11) Tripathi, S. K.; Pandey, K.; Rengasamy, K. R. R.; Biswal, B. K. Recent updates on the resistance mechanisms to epidermal growth factor receptor tyrosine kinase inhibitors and resistance reversion strategies in lung cancer. *Med. Res. Rev.* **2020**, *40* (6), 2132–2176.
- (12) da Rosa, R.; Schenkel, E. P.; Campos Bernardes, L. S. Semisynthetic and newly designed derivatives based on natural chemical scaffolds: Moving beyond natural products to fight *Trypanosoma cruzi*. *Phytochem. Rev.* **2020**, *19*, 105–122.
- (13) Tan, S.; Lu, R.; Yao, D.; Wang, J.; Gao, P.; Xie, G.; Liu, H.; Yao, X. Identification of LRRK2 Inhibitors through Computational Drug Repurposing. *ACS Chem. Neurosci.* **2023**, *14*, 481–493, DOI: 10.1021/acscchemneuro.2c00672.
- (14) Deng, J. N. Computer-Aided Drug Design. In *Current Drug Synthesis, 1st Edition*; Li, J. L., Ed.; 2022, pp 339–372. <https://doi.org/10.1002/9781119847281.ch18>
- (15) Lin, X.; Li, X.; Lin, X. A Review on Applications of Computational Methods in Drug Screening and Design. *Molecules* **2020**, *25* (6), No. 1375, DOI: 10.3390/molecules25061375.
- (16) Bertaccini, E. J. Anesthesia, Coming of Age in the World of Modern In Silico Drug Design. *Anesthesiology* **2023**, *138*, 129–131, DOI: 10.1097/aln.0000000000004445.
- (17) Cohen, N. C. *Guidebook on Molecular Modeling in Drug Design*; Gulf Professional Publishing, 1996.
- (18) Keith, J. A.; Vassilev-Galindo, V.; Cheng, B.; Chmiela, S.; Gastegger, M.; Müller, K.-R.; Tkatchenko, A. Combining machine learning and computational chemistry for predictive insights into chemical systems. *Chem. Rev.* **2021**, *121* (16), 9816–9872.
- (19) Moroy, G.; Martiny, V. Y.; Vayer, P.; Villoutreix, B. O.; Miteva, M. A. Toward in silico structure-based ADMET prediction in drug discovery. *Drug Discovery Today* **2012**, *17* (1–2), 44–55.
- (20) Tielens, F.; Gierada, M.; Handzlik, J.; Calatayud, M. Characterization of amorphous silica based catalysts using DFT computational methods. *Catal. Today* **2020**, *354*, 3–18.
- (21) Pracht, P.; Bohle, F.; Grimme, S. Automated exploration of the low-energy chemical space with fast quantum chemical methods. *Phys. Chem. Chem. Phys.* **2020**, *22* (14), 7169–7192.
- (22) Chalkha, M.; Nakkabi, A.; Hadda, T. B.; Berredjem, M.; Moussaoui, A. E.; Bakhouch, M.; Saadi, M.; Ammari, L. E.; Almalki, F. A.; Laaroussi, H.; Jevtovic, V.; Yazidi, M. E. Crystallographic study, biological assessment and POM/Docking studies of pyrazoles-sulfonamide hybrids (PSH): Identification of a combined Antibacterial/Antiviral pharmacophore sites leading to in-silico screening the anti-Covid-19 activity. *J. Mol. Struct.* **2022**, *1267*, No. 133605.
- (23) Elzahabi, H. S. A.; Nossier, E. S.; Alasfoury, R. A.; El-Manawaty, M.; Sayed, S. M.; Elkaeed, E. B.; Metwaly, A. M.; Hagra, M.; Eissa, I. H. Design, synthesis, and anti-cancer evaluation of new pyrido [2, 3-d] pyrimidin-4 (3H)-one derivatives as potential EGFRWT and EGFR790M inhibitors and apoptosis inducers. *J. Enzyme Inhib. Med. Chem.* **2022**, *37* (1), 1053–1076.
- (24) Sobh, E. A.; Dahab, M. A.; Elkaeed, E. B.; Alsouk, A. A.; Ibrahim, I. M.; Metwaly, A. M.; Eissa, I. H. Computer aided drug discovery (CADD) of a thieno[2,3-d]pyrimidine derivative as a new EGFR inhibitor targeting the ribose pocket. *J. Biomol. Struct. Dyn.* **2023**, *42*, 2369–2391, DOI: 10.1080/07391102.2023.2204500.
- (25) Elkaeed, E. B.; Yousef, R. G.; Elkady, H.; Alsouk, A. A.; Husein, D. Z.; Ibrahim, I. M.; Alswah, M.; Elzahabi, H. S.; Metwaly, A. M.; Eissa, I. H. A New Theobromine-Based EGFRWT and EGFR790M Inhibitor and Apoptosis Inducer: Design, Semi-Synthesis, Docking, DFT, MD Simulations, and In Vitro Studies. *Processes* **2022**, *10* (11), No. 2290, DOI: 10.3390/pr10112290.
- (26) Eissa, I. H.; Yousef, R. G.; Elkady, H.; Alsouk, A. A.; Alsouk, B. A.; Husein, D. Z.; Ibrahim, I. M.; Elkaeed, E. B.; Metwaly, A. M. A New Anticancer Semisynthetic Theobromine Derivative Targeting EGFR Protein: CADD Study. *Life* **2023**, *13* (1), No. 191, DOI: 10.3390/life13010191.
- (27) Eissa, I. H.; Yousef, R. G.; Elkaeed, E. B.; Alsouk, A. A.; Husein, D. Z.; Ibrahim, I. M.; Alesawy, M. S.; Elkady, H.; Metwaly, A. M. Anticancer derivative of the natural alkaloid, theobromine, inhibiting EGFR protein: Computer-aided drug discovery approach. *PLoS One* **2023**, *18* (3), No. e0282586.
- (28) Elkaeed, E. B.; Yousef, R. G.; Elkady, H.; Alsouk, A. A.; Husein, D. Z.; Ibrahim, I. M.; Metwaly, A. M.; Eissa, I. H. New anticancer theobromine derivative targeting egfrwt and egfr790m: Design, semi-synthesis, in silico, and in vitro anticancer studies. *Molecules* **2022**, *27* (18), No. 5859, DOI: 10.3390/molecules27185859.
- (29) Eissa, I. H.; Yousef, R. G.; Elkady, H.; Alsouk, A. A.; Husein, D. Z.; Ibrahim, I. M.; El-Deeb, N.; Kenawy, A. M.; Eldehna, W. M.; Elkaeed, E. B. New apoptotic anti-triple-negative breast cancer theobromine derivative inhibiting EGFRWT and EGFR790M: in silico and in vitro evaluation. *Mol. Diversity* **2023**, 1–21, DOI: 10.1007/s11030-023-10644-4.
- (30) Bonomi, P. Erlotinib: a new therapeutic approach for non-small cell lung cancer. *Expert Opin. Invest. Drugs* **2003**, *12* (8), 1395–1401.
- (31) Jänne, P. A.; Yang, J. C.-H.; Kim, D.-W.; Planchard, D.; Ohe, Y.; Ramalingam, S. S.; Ahn, M.-J.; Kim, S.-W.; Su, W.-C.; Horn, L.; et al. AZD9291 in EGFR inhibitor-resistant non-small-cell lung cancer. *N. Engl. J. Med.* **2015**, *372* (18), 1689–1699.
- (32) Elzahabi, H. S. A.; Nossier, E. S.; Alasfoury, R. A.; El-Manawaty, M.; Sayed, S. M.; Elkaeed, E. B.; Metwaly, A. M.; Hagra, M.; Eissa, I.

- H. Design, synthesis, and anti-cancer evaluation of new pyrido [2, 3-d] pyrimidin-4 (3H)-one derivatives as potential EGFRWT and EGFR-T790M inhibitors and apoptosis inducers. *J. Enzyme Inhib. Med. Chem.* **2022**, *37* (1), 1053–1076.
- (33) Gandin, V.; Ferrarese, A.; Via, M. D.; Marzano, C.; Chilin, A.; Marzaro, G. Targeting kinases with anilino-pyrimidines: discovery of N-phenyl-N'-[4-(pyrimidin-4-ylamino) phenyl] urea derivatives as selective inhibitors of class III receptor tyrosine kinase subfamily. *Sci. Rep.* **2015**, *5* (1), No. 16750, DOI: 10.1038/srep16750.
- (34) Liu, Y.; Gray, N. S. Rational design of inhibitors that bind to inactive kinase conformations. *Nat. Chem. Biol.* **2006**, *2* (7), 358–364.
- (35) Furet, P.; Caravatti, G.; Lydon, N.; Priestle, J. P.; Sowadski, J. M.; Trinks, U.; Traxler, P. Modelling study of protein kinase inhibitors: binding mode of staurosporine and origin of the selectivity of CGP 52411. *J. Comput.-Aided Mol. Des.* **1995**, *9* (6), 465–472.
- (36) Lipinski, C. A.; Lombardo, F.; Dominy, B. W.; Feeney, P. J. Experimental and computational approaches to estimate solubility and permeability in drug discovery and development settings. *Adv. Drug Delivery Rev.* **1997**, *23* (1–3), 3–25.
- (37) Chuang, K. V.; Gunsalus, L. M.; Keiser, M. J. Learning molecular representations for medicinal chemistry: miniperspective. *J. Med. Chem.* **2020**, *63* (16), 8705–8722.
- (38) Ferreira, L. L. G.; Andricopulo, A. D. ADMET modeling approaches in drug discovery. *Drug Discovery Today* **2019**, *24* (5), 1157–1165.
- (39) Idakwo, G.; Luttrell, J.; Chen, M.; Hong, H.; Zhou, Z.; Gong, P.; Zhang, C. A review on machine learning methods for in silico toxicity prediction. *J. Environ. Sci. Health, Part C* **2018**, *36* (4), 169–191.
- (40) Kruhlak, N. L.; Benz, R. D.; Zhou, H.; Colatsky, T. J. (Q)SAR modeling and safety assessment in regulatory review. *Clin. Pharmacol. Ther.* **2012**, *91* (3), 529–534.
- (41) Tice, R. R.; Bassan, A.; Amberg, A.; Anger, L. T.; Beal, M. A.; Bellion, P.; Benigni, R.; Birmingham, J.; Brigo, A.; Bringezu, F.; Ceriani, L.; Crooks, I.; Cross, K.; Elespuru, R.; Faulkner, D. M.; Fortin, M. C.; Fowler, P.; Frericks, M.; Gerets, H. H. J.; Jahne, G. D.; Jones, D. R.; Kruhlak, N. L.; Lo Piparo, E.; Lopez-Belmonte, J.; Lunival, A.; Luu, A.; Madia, F.; Manganelli, S.; Manickam, B.; Mestres, J.; Mihalchik-Burhans, A. L.; Neilson, L.; Pandiri, A.; Pavan, M.; Rider, C. V.; Rooney, J. P.; Trejo-Martin, A.; Watanabe-Sailor, K. H.; White, A. T.; Woolley, D.; Myatt, G. J. In Silico Approaches In Carcinogenicity Hazard Assessment: Current Status and Future Needs. *Comput. Toxicol.* **2021**, *20*, No. 100191, DOI: 10.1016/j.comtox.2021.100191.
- (42) Xu, C.; Cheng, F.; Chen, L.; Du, Z.; Li, W.; Liu, G.; Lee, P. W.; Tang, Y. In silico prediction of chemical Ames mutagenicity. *J. Chem. Inf. Model.* **2012**, *52* (11), 2840–2847.
- (43) Thresher, A.; Gosling, J. P.; Williams, R. Generation of TD(50) values for carcinogenicity study data. *Toxicol. Res.* **2019**, *8* (5), 696–703.
- (44) Stampfer, H. G.; Gabb, G. M.; Dimmitt, S. B. Why maximum tolerated dose? *Br. J. Clin. Pharmacol.* **2019**, *85* (10), 2213–2217.
- (45) Lane, T. R.; Harris, J.; Urbina, F.; Ekins, S. Comparing LD(50)/LC(50) Machine Learning Models for Multiple Species. *ACS Chem. Health Saf.* **2023**, *30* (2), 83–97.
- (46) Gadaleta, D.; Marzo, M.; Toropov, A.; Toropova, A.; Lavado, G. J.; Escher, S. E.; Dorne, J. L. C. M.; Benfenati, E. Integrated In Silico Models for the Prediction of No-Observed-(Adverse)-Effect Levels and Lowest-Observed-(Adverse)-Effect Levels in Rats for Sub-chronic Repeated-Dose Toxicity. *Chem. Res. Toxicol.* **2021**, *34* (2), 247–257.
- (47) Husein, D. Z.; Hassanien, R.; Khamis, M. Cadmium oxide nanoparticles/graphene composite: Synthesis, theoretical insights into reactivity and adsorption study. *RSC Adv.* **2021**, *11* (43), 27027–27041.
- (48) Wang, T.; Husein, D. Z. Novel synthesis of multicomponent porous nano-hybrid composite, theoretical investigation using DFT and dye adsorption applications: Disposing of waste with waste. *Environ. Sci. Pollut. Res.* **2023**, *30*, 8928–8955.
- (49) Liu, X.; Shi, D.; Zhou, S.; Liu, H.; Liu, H.; Yao, X. Molecular dynamics simulations and novel drug discovery. *Expert Opin. Drug Discovery* **2018**, *13* (1), 23–37.
- (50) De Vivo, M.; Masetti, M.; Bottegioni, G.; Cavalli, A. Role of molecular dynamics and related methods in drug discovery. *J. Med. Chem.* **2016**, *59* (9), 4035–4061.
- (51) Abraham, M. J.; Murtola, T.; Schulz, R.; Páll, S.; Smith, J. C.; Hess, B.; Lindahl, E. GROMACS: High performance molecular simulations through multi-level parallelism from laptops to supercomputers. *SoftwareX* **2015**, *1-2*, 19–25.
- (52) Brooks, B. R.; Brooks, C. L., III; Mackerell, A. D., Jr; Nilsson, L.; Petrella, R. J.; Roux, B.; Won, Y.; Archontis, G.; Bartels, C.; Boresch, S.; et al. CHARMM: the biomolecular simulation program. *J. Comput. Chem.* **2009**, *30* (10), 1545–1614.
- (53) Valdés-Tresanco, M. S.; Valdés-Tresanco, M. E.; Valiente, P. A.; Moreno, E. gmx_MMPBSA: a new tool to perform end-state free energy calculations with GROMACS. *J. Chem. Theory Comput.* **2021**, *17* (10), 6281–6291.
- (54) Xiong, G.; Shen, C.; Yang, Z.; Jiang, D.; Liu, S.; Lu, A.; Chen, X.; Hou, T.; Cao, D. Featurization strategies for protein–ligand interactions and their applications in scoring function development. *Comput. Mol. Biosci.* **2022**, *12* (2), No. e1567, DOI: 10.1002/wcms.1567.
- (55) Zhao, Z.; Bourne, P. E. Harnessing systematic protein–ligand interaction fingerprints for drug discovery. *Drug Discovery Today* **2022**, *27*, No. 103319, DOI: 10.1016/j.drudis.2022.07.004.
- (56) Bouysset, C.; Fiorucci, S. ProLIF: a library to encode molecular interactions as fingerprints. *J. Cheminf.* **2021**, *13*, No. 72, DOI: 10.1186/s13321-021-00548-6.
- (57) Salentin, S.; Adasme, M. F.; Heinrich, J. C.; Haupt, V. J.; Daminelli, S.; Zhang, Y.; Schroeder, M. From malaria to cancer: Computational drug repositioning of amodiaquine using PLIP interaction patterns. *Sci. Rep.* **2017**, *7* (1), No. 11401.
- (58) Salentin, S.; Schreiber, S.; Haupt, V. J.; Adasme, M. F.; Schroeder, M. PLIP: fully automated protein–ligand interaction profiler. *Nucleic Acids Res.* **2015**, *43* (W1), W443–W447.
- (59) Tubiana, T.; Carvillat, J.-C.; Boulard, Y.; Bressanelli, S. Modeling, TTClust: a versatile molecular simulation trajectory clustering program with graphical summaries. *J. Chem. Inf.* **2018**, *58* (11), 2178–2182.
- (60) Papaleo, E.; Mereghetti, P.; Fantucci, P.; Grandori, R.; De Gioia, L. Free-energy landscape, principal component analysis, and structural clustering to identify representative conformations from molecular dynamics simulations: the myoglobin case. *J. Mol. Graphics Modell.* **2009**, *27* (8), 889–899.
- (61) David, C. C.; Jacobs, D. J. Principal Component Analysis: A Method for Determining the Essential Dynamics of Proteins. In *Protein Dynamics: Methods Protocols*; Springer, 2014.
- (62) Maisuradze, G. G.; Leitner, D. M. Free energy landscape of a biomolecule in dihedral principal component space: Sampling convergence and correspondence between structures and minima. *Proteins: Struct., Funct., Bioinf.* **2007**, *67* (3), 569–578.
- (63) Hess, B. Similarities between principal components of protein dynamics and random diffusion. *Phys. Rev. E* **2000**, *62* (6), No. 8438, DOI: 10.1103/PhysRevE.62.8438.
- (64) Eissa, I. H.; Yousef, R. G.; Elkady, H.; Alsouk, A. A.; Alsouk, B. A.; Husein, D. Z.; Ibrahim, I. M.; Elkaeed, E. B.; Metwaly, A. M. A New Anticancer Semisynthetic Theobromine Derivative Targeting EGFR Protein: CADD Study. *Life* **2023**, *13* (1), No. 191, DOI: 10.3390/life13010191.
- (65) Obeng, E. Apoptosis (programmed cell death) and its signals-A review. *Braz. J. Biol.* **2021**, *81*, 1133–1143.
- (66) Wyllie, A. H. Glucocorticoid-induced thymocyte apoptosis is associated with endogenous endonuclease activation. *Nature* **1980**, *284*, 555–556.
- (67) Alanazi, M. M.; Eissa, I. H.; Alsaif, N. A.; Obaidullah, A. J.; Alanazi, W. A.; Alasmari, A. F.; Albassam, H.; Elkady, H.; Elwan, A. Design, synthesis, docking, ADMET studies, and anticancer evaluation of new 3-methylquinoxaline derivatives as VEGFR-2

inhibitors and apoptosis inducers. *J. Enzyme Inhib. Med. Chem.* **2021**, *36* (1), 1760–1782.

(68) Porter, A. G.; Jänicke, R. U. Emerging roles of caspase-3 in apoptosis. *Cell Death Differ.* **1999**, *6* (2), 99–104.

(69) Li, P.; Zhou, L.; Zhao, T.; Liu, X.; Zhang, P.; Liu, Y.; Zheng, X.; Li, Q. Caspase-9: structure, mechanisms and clinical application. *Oncotarget* **2017**, *8* (14), 23996–24008, DOI: 10.18632/oncotarget.15098.

(70) Shacter, E.; Weitzman, S. A. Chronic inflammation and cancer. *Oncology* **2002**, *16* (2), 217–226.

(71) Angelo, L. S.; Kurzrock, R. Vascular endothelial growth factor and its relationship to inflammatory mediators. *Clin. Cancer Res.* **2007**, *13* (10), 2825–2830.

(72) Roberti, M. P.; Barrio, M. M.; Bravo, A.; Rocca, Y.; Arriaga, J. M.; Bianchini, M.; Mordoh, J.; Levy, E. M. J. B. c. r. IL-15 and IL-2 increase Cetuximab-mediated cellular cytotoxicity against triple negative breast cancer cell lines expressing EGFR. *Breast Cancer Res. Treat.* **2011**, *130*, 465–475, DOI: 10.1007/s10549-011-1360-2.

(73) Shibuya, H.; Yoneyama, M.; Ninomiya-Tsuji, J.; Matsumoto, K.; Taniguchi, T. IL-2 and EGF receptors stimulate the hematopoietic cell cycle via different signaling pathways: demonstration of a novel role for c-myc. *Cell* **1992**, *70* (1), 57–67.

(74) Lee, C.-W.; Lin, C.-C.; Lin, W.-N.; Liang, K.-C.; Luo, S.-F.; Wu, C.-B.; Wang, S.-W.; Yang, C.-M. TNF- α induces MMP-9 expression via activation of Src/EGFR, PDGFR/PI3K/Akt cascade and promotion of NF- κ B/p300 binding in human tracheal smooth muscle cells. *Am. J. Physiol.: Lung Cell. Mol. Physiol.* **2007**, *292* (3), L799–L812.

(75) Suleimen, Y. M.; Jose, R. A.; Mamytbekova, G. K.; Suleimen, R. N.; Ishmuratova, M. Y.; Dehaen, W.; Alsouk, B. A.; Elkaeed, E. B.; Eissa, I. H.; Metwaly, A. M. Isolation and In Silico Inhibitory Potential against SARS-CoV-2 RNA Polymerase of the Rare Kaempferol 3-O-(6"-O-acetyl)-Glucoside from *Calligonum tetrapterum*. *Plants* **2022**, *11* (15), No. 2072, DOI: 10.3390/plants11152072.

(76) Jo, S.; Cheng, X.; Islam, S. M.; Huang, L.; Rui, H.; Zhu, A.; Lee, H. S.; Qi, Y.; Han, W.; Vanommeslaeghe, K. et al. CHARM-GUI PDB manipulator for advanced modeling and simulations of proteins containing nonstandard residues. In *Advances in Protein Chemistry Structural Biology*; Elsevier, 2014.

(77) Valdés-Tresanco, M. S.; Valdés-Tresanco, M. E.; Valiente, P. A.; Moreno, E. gmx_MMPBSA: A New Tool to Perform End-State Free Energy Calculations with GROMACS. *J. Chem. Theory Comput.* **2021**, *17* (10), 6281–6291, DOI: 10.1021/acs.jctc.1c00645.

(78) Amadei, A.; Linssen, A. B.; Berendsen, H. J. Essential dynamics of proteins. *Proteins: Struct., Funct., Bioinf.* **1993**, *17* (4), 412–425.

(79) Systèmes, Dassault. "Biovia, discovery studio modeling environment." Dassault Systèmes Biovia: San Diego, CA, USA (2017).

(80) Yousef, R. G.; Elwan, A.; Gobaara, I. M.; Mehany, A. B.; Eldehna, W. M.; El-Metwally, S. A.; A Alsouk, B.; Elkaeed, E. B.; Metwaly, A. M.; Eissa, I. H. Anti-cancer and immunomodulatory evaluation of new nicotinamide derivatives as potential VEGFR-2 inhibitors and apoptosis inducers: in vitro and in silico studies. *J. Enzyme Inhib. Med. Chem.* **2022**, *37* (1), 2206–2222, DOI: 10.1080/14756366.2022.2110868.

(81) Alley, M. C.; Scudiero, D. A.; Monks, A.; Hursey, M. L.; Czerwinski, M. J.; Fine, D. L.; Abbott, B. J.; Mayo, J. G.; Shoemaker, R. H.; Boyd, M. R. Feasibility of drug screening with panels of human tumor cell lines using a microculture tetrazolium assay. *Cancer Res.* **1988**, *48* (3), 589–601.

(82) Van de Loosdrecht, A.; Beelen, R.; Ossenkoppele, g.; Broekhoven, M.; Langenhuijsen, M. A tetrazolium-based colorimetric MTT assay to quantitate human monocyte mediated cytotoxicity against leukemic cells from cell lines and patients with acute myeloid leukemia. *J. Immunol. Methods* **1994**, *174* (1–2), 311–320.

(83) Koch, A.; Tamez, P.; Pezzuto, J.; Soejarto, D. Evaluation of plants used for antimalarial treatment by the Maasai of Kenya. *J. Ethnopharmacol.* **2005**, *101* (1–3), 95–99.